Review Article

Enhanced Photocatalytic Degradation of Methylene Blue and Methyl Orange Dyes via Transition Metal-Doped Titanium Dioxide Nanoparticles

Abstract

Herein, we reviewed the photocatalytic degradation of methylene blue and methyl orange using titanium dioxide nanoparticles.The nanoparticles normally face challenges due to electron-hole recombination effects and low surface area. Doping with transition metals such as copper (Cu), chromium (Cr), manganese (Mn), cobalt (Co) and nickel (Ni) is an alternative way of reducing the electron-hole recombination effects, improves structural and electronic properties but also reduces on the band gap energy below 3.0 eV. Photocatalyst which is an advanced oxidation process (AOP) is used as an alternative to remove both methylene blue and methyl orange dyes. This process produces highly reactive oxygen species (ROS) such as hydroxyl radical, sulphates and superoxide radical which create alternative pathways for the degradation of synthetic dyes to less toxic by-products which are water, hydrochloric acid and carbondioxide. This review further discusses the synthesis techniques which include chemical vapor deposition, hydrothermal synthesis, sonochemical synthesis, sol-gel method, spray pyrolysis, etc that are commonly used in the preparation of pure and doped titanium dioxide nanoparticles.

Keywords: photocatalysis, titanium dioxide, methylene blue, methyl orange, sol-gel.

1. INTRODUCTION

The increase in industrialization and the need for cheap energy sources globally has seen a rise in the contamination of the earth's water bodies[1]. The industries associated with this rapid increase include paper making, paint factories, food processing, and textile dyeing[2–4].Industrial waste effluents contain a number of both inorganic and organic pollutants which include toxic heavy metals, pesticides, pharmaceuticals, and dyes[5].Dyes are chemical species that normally connect to the fabric of material to impart different colors [6]. It has been reported that about 700,000 tons per year of various dyes from different colors are produced commercially from the available 100,000 natural and synthetic dyes [6].Textile dyes that are

directly discharged into the water bodies include methyl orange, methylene blue, malachite green, crystal violet etc.These dyes are non-biodegradable, carcinogenic, and reduce the esthetic nature of the aqueous environment thus posing a threat to both aquatic and human life[7–11].The reactive dyes have been observed to have different functional groups onto which they attach to the surface of the substrate hence a challenge during water treatment[12].

The treatment of dye-contaminated water follows four techniques i.e. physiochemical, biological, physical, and chemical water treatment methods. Among these separation techniques the most adopted include adsorption, biodegradation, membrane filtration, coagulation, reverse osmosis and advanced oxidation processes (AOPs) have been used in the removal of these dyes[13–15]. Adsorption is the most commonly used wastewater treatment technique due to its simplicity in design, low cost, and availability [16]. However, it has some drawbacks such as the creation of secondary toxicity, mechanical instability of the adsorbent but also low adsorption efficacy [17]. Advanced oxidation processes are generally defined as oxidation technologies that involve the in-situ generation of hydroxyl radicals that are highly reactive and are used in the degradation of pollutants of emerging concern [18–20].AOPS are being used as alternatives since they remove about 96 % of colored compounds compared to 49 % when adsorption is used for treatment [21,22]. AOPs are used because they have many advantages such as high mineralization, do not create secondary toxicity, and rapid oxidation reaction rate [23–26].TheAOPs which include sonochemical oxidation, photocatalytic oxidation, Fenton reactions, electrochemical oxidation reactions, and sulphate radical-based AOPs (SR-AOPs) are known to generate highly reactive radicals that degrade organic pollutants. The AOPs have been observed to mineralize organic pollutants through the ability to generate reactive oxygen species (ROS) which include the hydroxyl radical (·OH) [23,27], sulphates[28], and superoxide radical ($\cdot O_2^-$)[28]. AOPs are divided into two main categories i.e. heterogeneous and homogenous catalysis[29]. Heterogeneous catalysts have been successfully applied in environmental remediation through the degradation of hazardous organic pollutants.Titanium dioxide (TiO_2) which is a heterogeneous photocatalyst, non-toxic, inexpensive, and highly reactive has been widely applied in the photodegradation of synthetic dyes [30–32]. Titanium dioxide is known to mineralize dyes into carbon dioxide (CO_2), water, and HCl as such it does not produce toxic intermediates but also the reaction occurs at room temperature[33–35].However, Titanium dioxide faces a number of drawbacks such as electron-hole recombination which reduces

quantum efficiency, low surface area which results in ineffective pollutant degradation but also low ability to absorb visible light which restricts technological application[36]. Thus, to improve visible light absorption, a number of modifications have been carried out such as doping with metals and non-metals, dye sensitization, and coupling with other semiconductors. Doping with transition metals reduces the recombination effects of the electrons and holes thus improving the photocatalytic activity of TiO_2 nanoparticles [37]. This review aims to describe the photocatalytic degradation of methylene blue and methyl orange dyes using both doped and undoped titanium dioxide nanoparticles.It also introduces the different synthetic techniques for the fabrication of TiO_2 nanoparticles. It will further illustrate the characterization techniques of the different titanium dioxide nanostructures and how they influence the degradation of the dyes to less harmful by-products.

2. SYNTHETIC DYES

A dye is known as a synthetic or natural substance that when introduced into a medium interacts with it through dispersion and dissolving in it[38]. They are applied in textiles due to the ability to be fixed onto fabric but also absorption of a wide spectrum of colors from light. Dyes have a chemical structure made up of three components which include chromophores (give the dye color), auxochrome (enable fixation onto the substrate), and solubilizing groups (enhance solubility in organic and aqueous solvents)[39,40]. The chromophore consists of a number of groups such as the nitro, nitroso, carbonyl, azo, alkenes, and thiocarbonyl [41]. Figure 1 shows the different molecules containing chromophores and auxochromes.

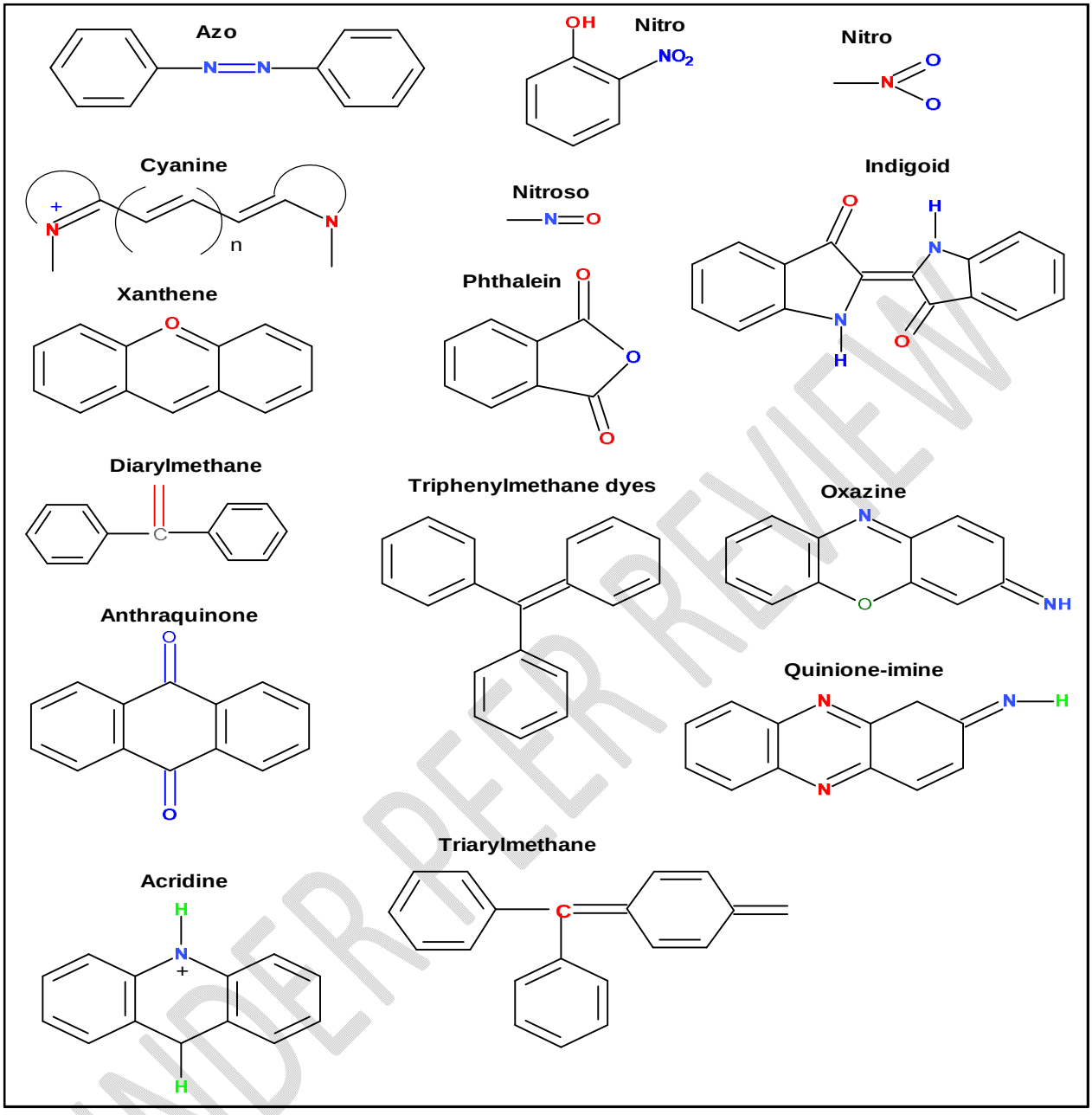

Fig 1. A schematic representation of dyes according to chromophores.

The auxochromes that enable the fixation of the dye but also its modification maybe acidic (SO_3 or COOH) or basic (NR_2, NH_2, or NHR) in nature[42]. A molecule that contains both the chromophore and auxochrome is known as a chromogen[43].In brief, dyes contain several chromophoric, auochromic groups and conjugated systems (anthracene, benzene, perylene, etc). There are about 8000 different synthetic dyes classified as either ionic or non-ionic as shown in

Figure 2. The ionic dyes are further divided into anionic and cationic while the non-ionic are subdivided into Vat and Disperse dyes[44].

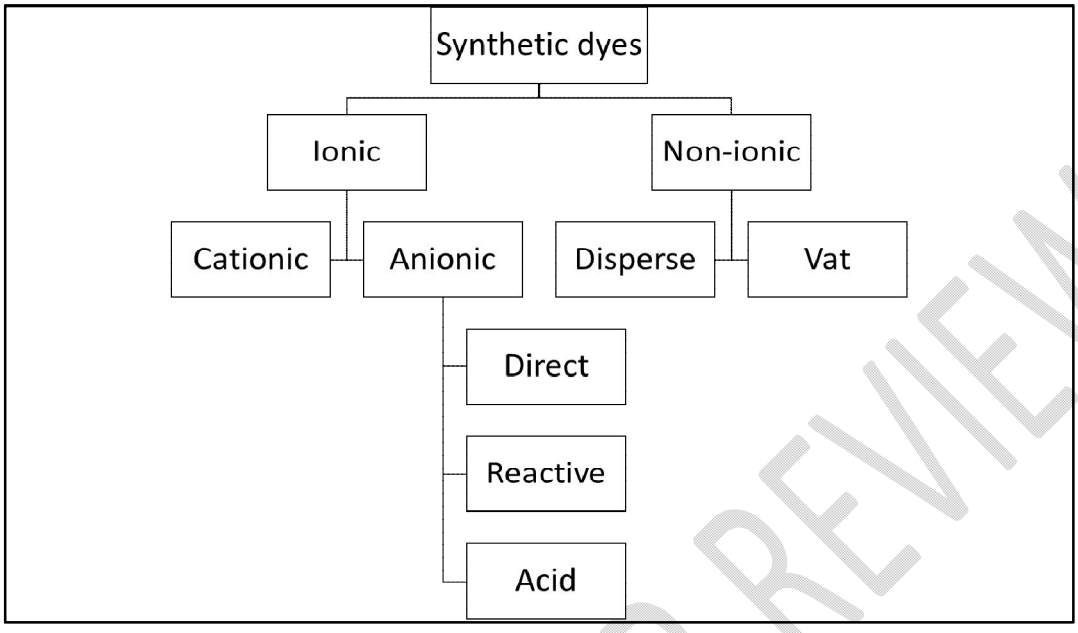

Fig 2. A classification of the synthetic dyes.

Acid dyes are anionic sulfonated dyes with one or more acid functions with a high affinity for basic fibers such as polyamides[43]. The majority of these dyes are applied on nylon, cotton, polyamides and they constitute about 30-40 % of the total dye consumption[45,46]. Because of the bright colors and high solubility, these dyes are widely applied in textile, printing, pharmaceutical, and leather factories[47]. Figure 3 shows some of the common acid dyes.

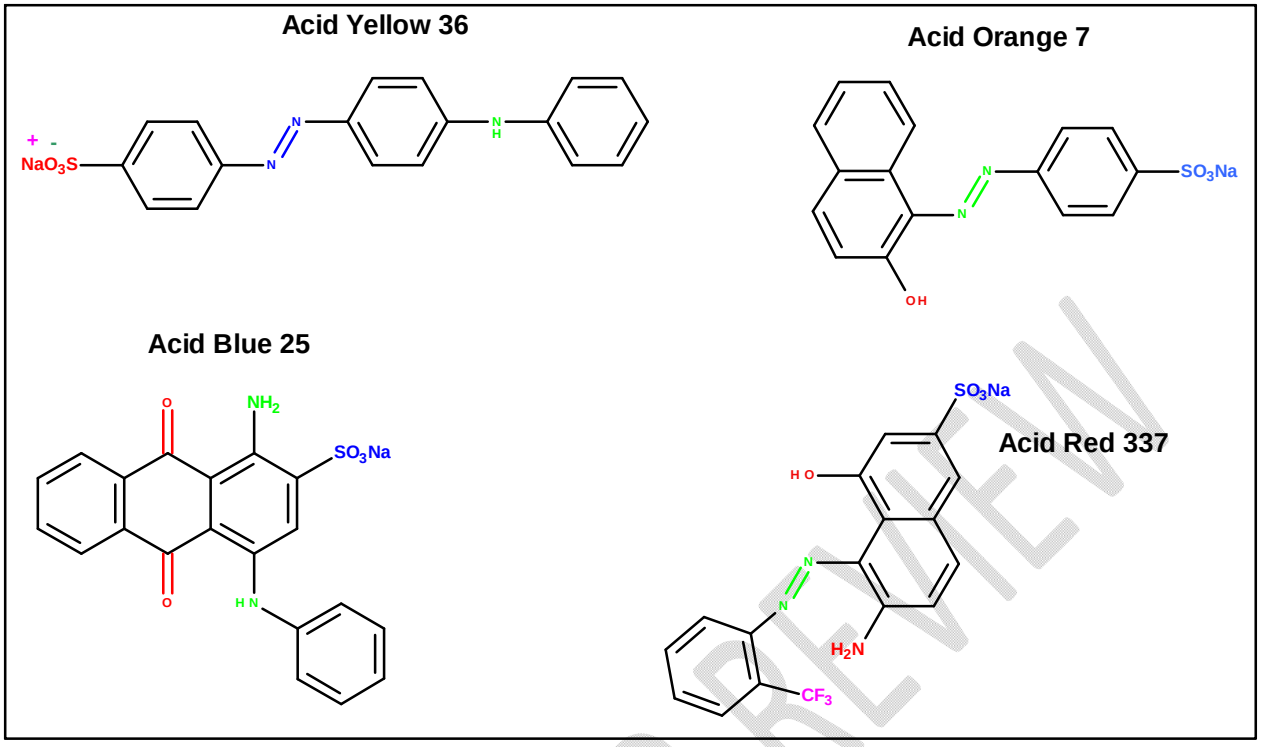

Fig 3. Chemical structures of some of the acid dyes

Reactive dyes are soluble anionic dyes, that tend to be repelled by cotton fabric that has a negatively charged surface[48]. These dyes have a low degradability and are highly soluble in water. With a variation in profile shades, vivid colors, colorfastness, and photolytic stability, reactive dyes have seen tremendous application in the synthetic industry[38,49,50]. It is the most applied dye when it comes to cellulosic fibers but also in proteins like silk and wool[51]. Figure 4 shows the most common reactive dyes.

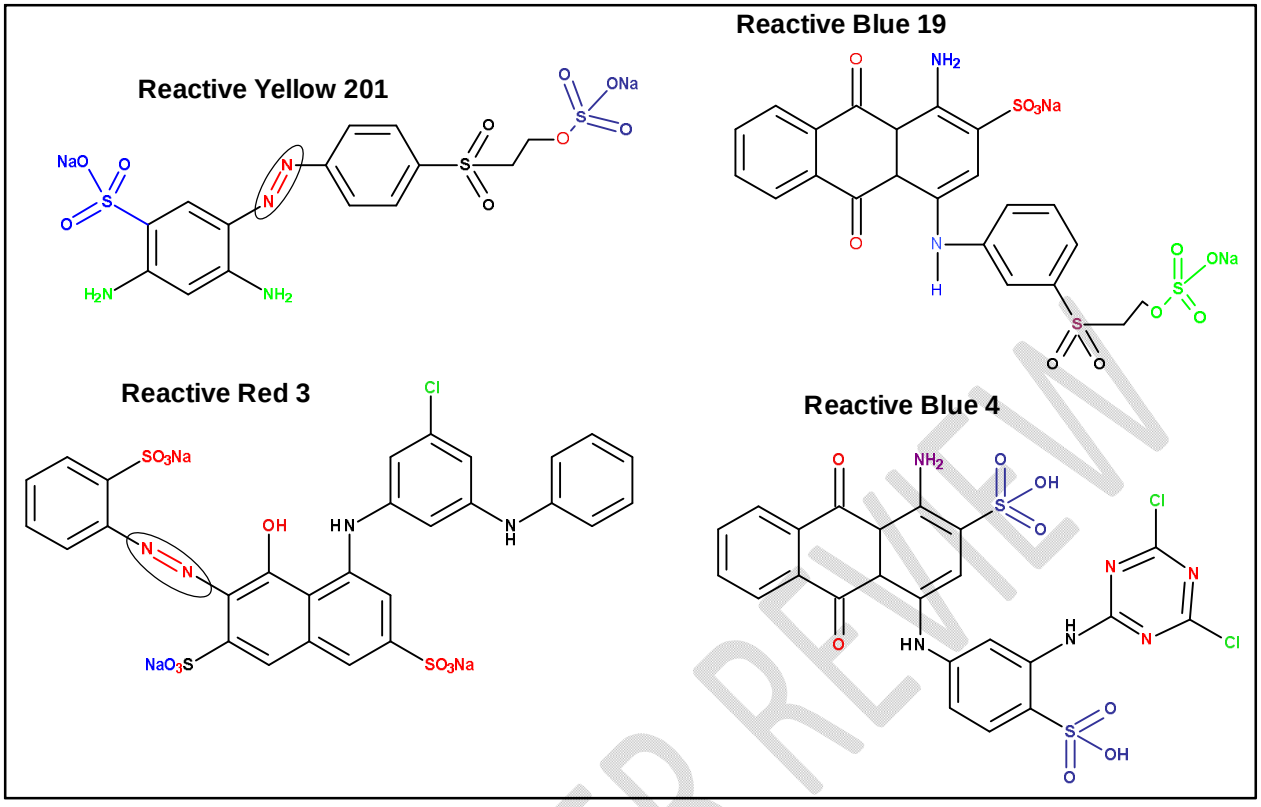

Fig 4. Chemical structures of some of the reactive dyes.

Direct dyes are anionic, water soluble and are widely used in the textile industries due to their being cheap and economic factors[52]. They loosely bind with the fabric of the substrate, do not dry up easily, and are applied at a temperature of 79.4 – 93.3 °C[53]. These dyes are observed to have the tendency to be cold-washed because they have low fixation properties[54]. Some examples of the direct dyes are shown in Figure 5.

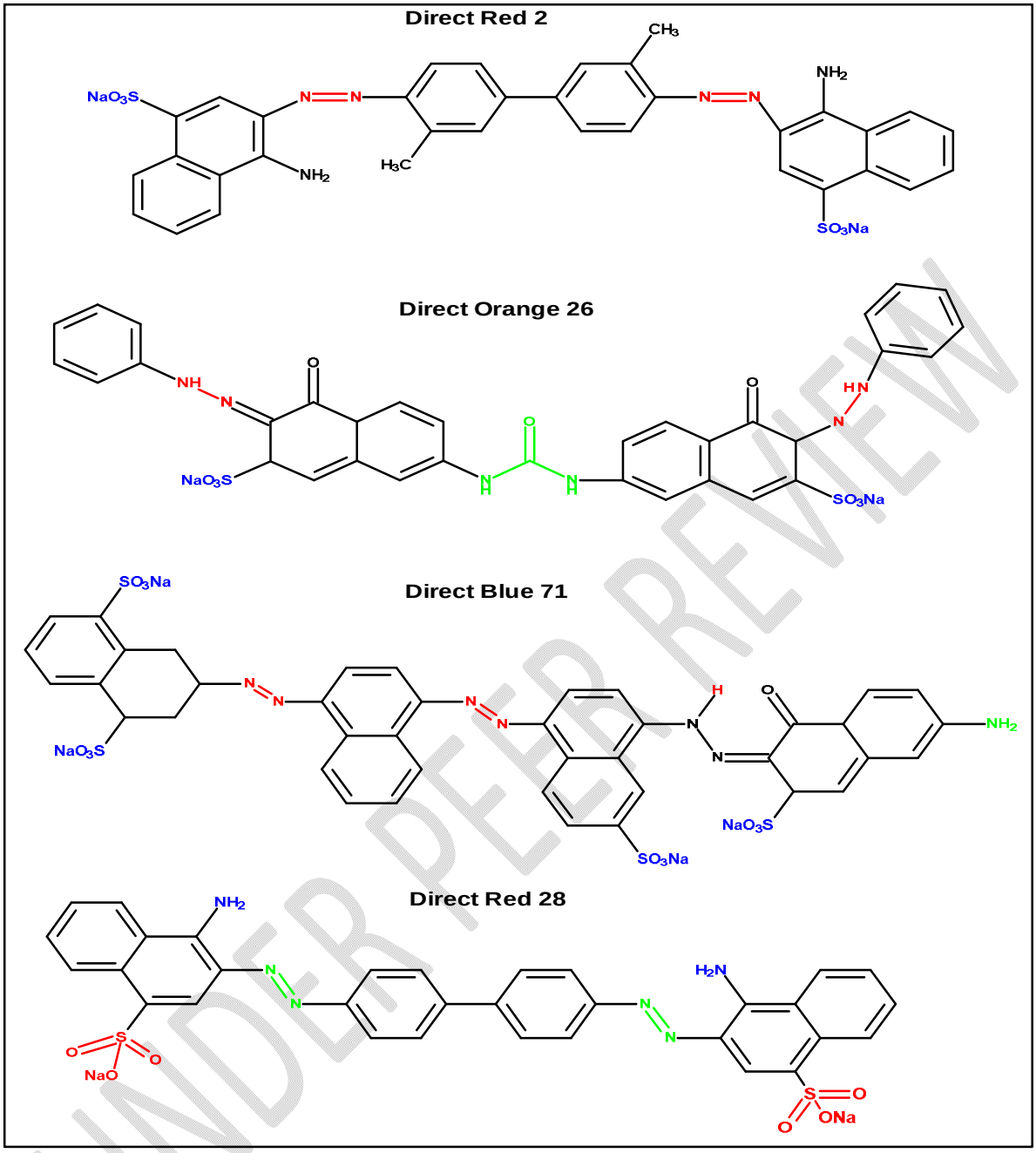

Fig 5. Chemical structures of some of the direct dyes.

Vat dyesare reported to have excellent brightness properties but also colorfastness making them easily identifiable[55]. They are also known to be soluble in water but also some dissolve in sodium carbonate[54]. It is the most applied dye in the coloration of cotton substrate and it represents 24 % of the cellulose fiber dye market[56,57].Vat dyes are held to cellulose through

hydrogen bonding and van der Waal forces of attraction[58]. Some of the Vat dyes are illustrated in Figure 6.

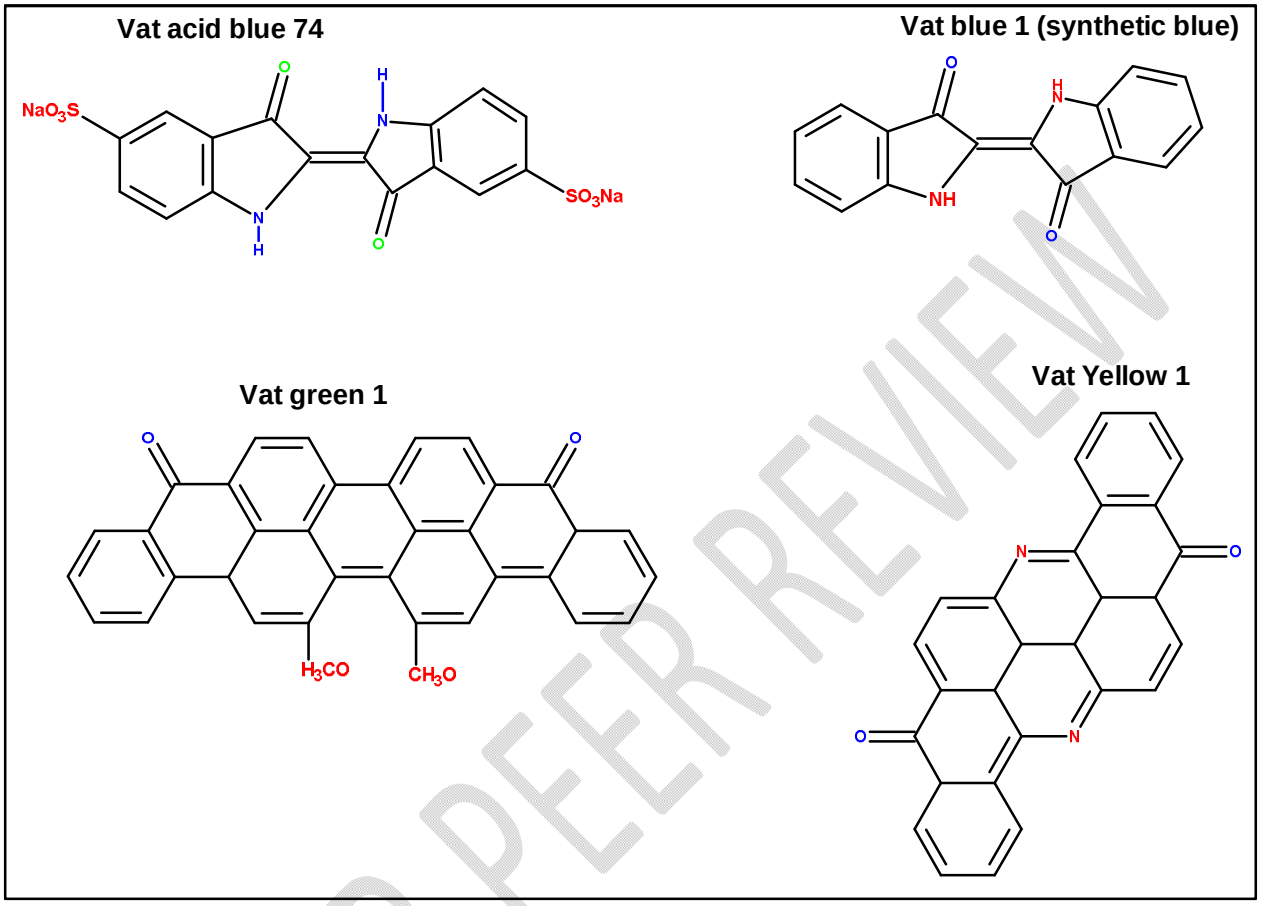

Fig 6. Chemical structures of some of the vat dyes.

Disperse dyes are non-ionic, colored, insoluble in water, contain either nitro or azo groups, and are widely used in the dyeing of synthetic fiber in an aqueous dispersion[59]. They represent about 44 % of the total dye produced and are normally applied to hydrophobic fibers[60,61]. Furthermore, they are known to be persistent and non-biodegradable[62]. Figure 7 shows some of the commonly applied disperse dyes.

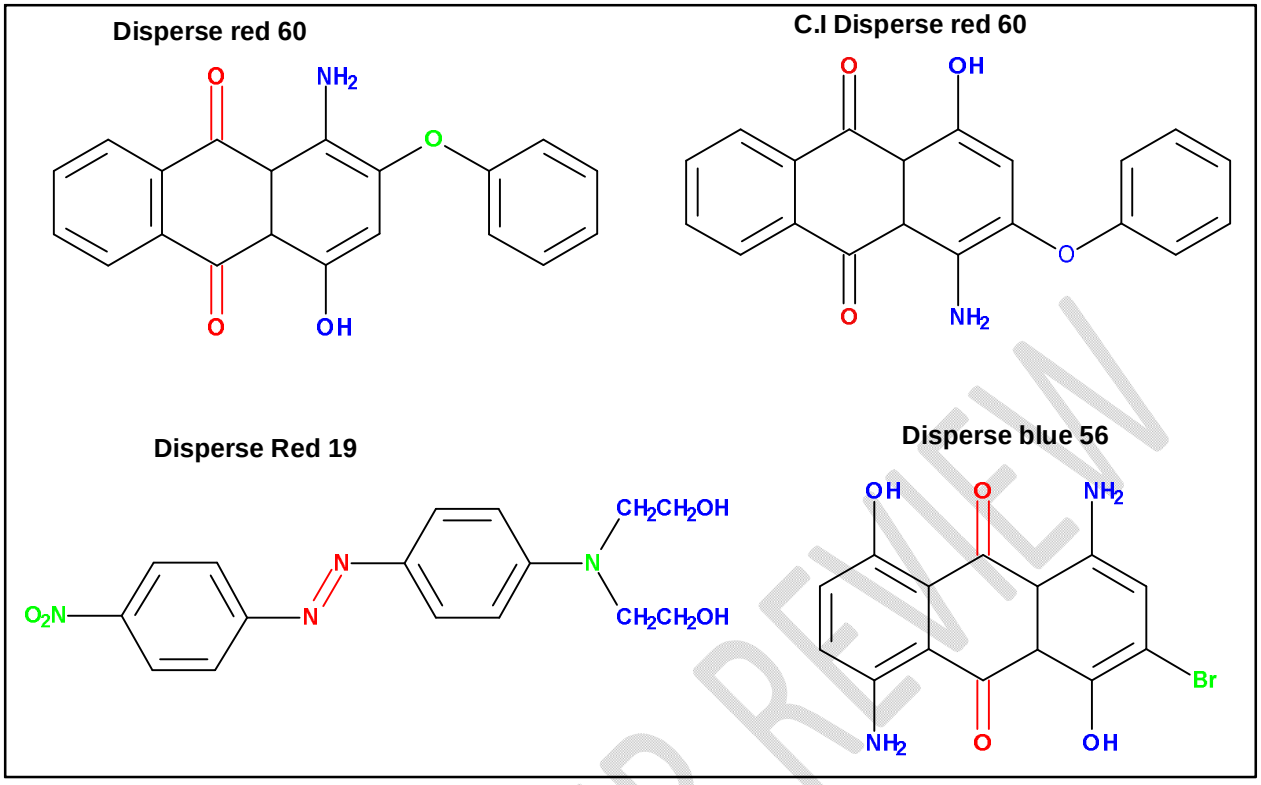

Fig 7. Chemical structures of some of the disperse dyes.

3. TITANIUM DIOXIDE

Titanium diode also known as titania is a transition metal oxide that naturally occurs and has a chemical formula of TiO_2[63]. It is a white pigment normally found in crayons, paint, electronic components, cosmetics, rubber, plastics, and synthetic fibers. It is a semiconductor material having a band gap of 3.2 eV corresponding to a wavelength of 390 nm [64]. Figure 8 shows the three crystalline forms ofTitanium dioxide that are rutile, brookite, and anatase phases[65].

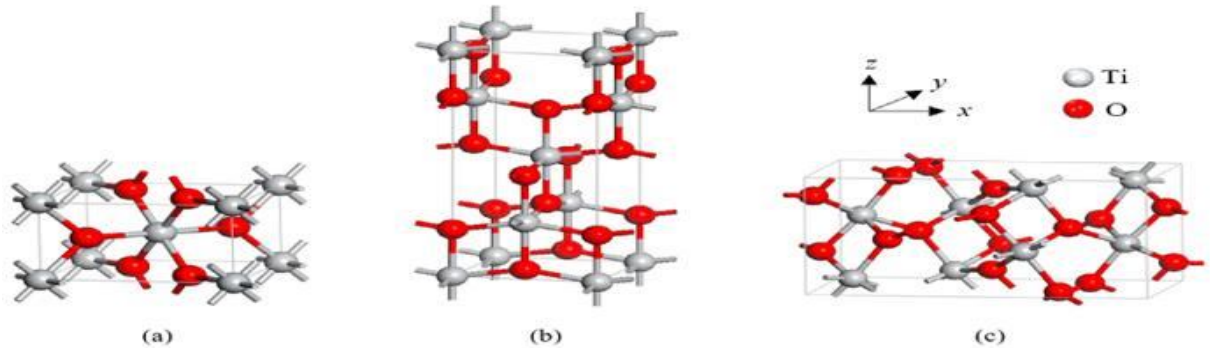

Fig 8. A cell unit of rutile, anatase and brookite TiO_2 crystalline phases [66].

Anatase phase is considered to have the highest photocatalytic activities since it has some crystallographic planes that are reactive [67,68]. However numerous studies have been done which describe the rutile form to have comparable photocatalytic activity with that of anatase [69–71]. Due to an increase in research on surface chemistry, TiO_2 has seen rapid applications such as in coatings, photovoltaics, photocatalysis, photoelectrochemical cells, and sensors[72–76]. This rapid growth has been observed in the fields of nanoscience and nanotechnology due to the production of nanosized materials[77].Titanium dioxide nanoparticles in the nanometer range have been applied in the photocatalytic degradation of organic pollutants, especially synthetic dyes[78–81]. The nanoparticles have an efficiency that can be modified for more efficient photocatalytic degradation. Doping with different metals and non-metals is a better alternative which is encouraged to improve the photocatalytic activity of the nanoparticles.

3.1 PHOTOCATALYTIC REACTIONS USING TiO_2

Photocatalytic reactions are widely studied to describe the degradation of organic pollutants at operational temperature and pressure through mineralization resulting in the generation of less toxic products. TiO_2 will be used as the model to describe the photocatalytic mechanism for the degradation of organic pollutants. Three equations describe the photocatalytic degradation of organic pollutants. In the first stage,TiO_2 undergoes photo excitation which causes photoinduction of electrons. The energy of the photon must be greater than the band gap thus facilitating the generation of electrons (e^-) and holes (h^+) as shown in Equation 1.

$$TiO_2 + h\nu \rightarrow e^- + h^+ \quad (1)$$

The generated electron (e^-) due to photoexcitation through band transitions moves from the valence band to the conduction band. Due to the migration of the electrons to the conduction band, this creates holes (h^+) in the valence band.

During the second stage, the holes and the photoinduced electrons react with H_2O and O_2 to form highly reactive hydroxyl radical and superoxide radical ($\cdot O_2^-$). The O_2 adsorbed on the surface of the photocatalyst reacts with the electron to form the superoxide radical ($\cdot O_2^-$) as shown in Equation 2.

$$O_2 + e^- \rightarrow \cdot O_2^- \quad (2)$$

The radical then reacts with H_2O to form the hydroperoxyl radical ($HO_2^{\cdot}$) as shown in Equation 3.

$$\cdot O_2^- + H_2O \rightarrow HO_2^{\cdot} \quad (3)$$

The holes oxidize H_2O and OH^- to generate the reactive hydroxyl radical as shown in Equation 4.

$$H_2O/OH^- + h^+ \rightarrow \cdot OH \quad (4)$$

Lastly, the third stage is where the reactive hydroxyl radical, superoxide radical, and hydroperoxyl radical react with the organic pollutants (OPs) to generate carbon dioxide and water which are environmentally friendly by-products as shown in Equation 5.

$$(\cdot O_2^-)/(HO_2^{\cdot})/\cdot OH + OPs \rightarrow CO_2 + H_2O \quad (5)$$

Figure 9illustrates the whole photocatalytic mechanism for the degradation of organic pollutants using TiO_2 semiconductors.

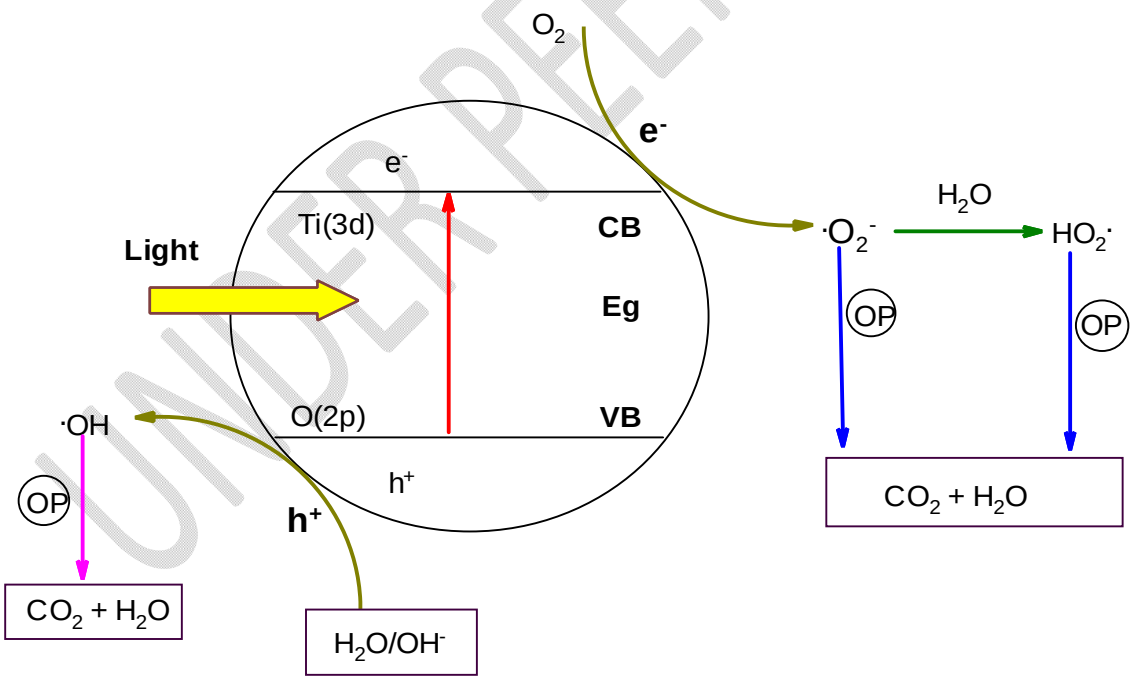

Fig 9. Photocatalytic Mechanism for degradation of organic pollutants.

3.2 PREPARATION AND CHARACTERIZATION OF TITANIUM DIOXIDE NANOSTRUCTURES

Titanium dioxide nanostructures are synthesized using a number of techniques as will be discussed in this review. The method of synthesis greatly influences some factors such as the morphology, surface area, and surface vacancy sites but also photocatalytic activity. The commonly used methods include hydrothermal synthesis, sol-gel, micelle method, solvothermal synthesis, anodization, flame spray pyrolysis, electrospinning, microwave-assisted, thermal oxidation, direct oxidation, spray pyrolysis, pulsed laser deposition, sonochemical synthesis, spin coating, atomic layer deposition, and electrochemical deposition. Synthesis of TiO_2 nanoparticles is based on a variety of precursors which include titanium trichloride ($TiCl_3$), titanium isopropoxide (TTIP), titanium tetrachloride ($TiCl_4$), and titanium tetrabutoxide (TBT)[82–84].

Hydrothermal synthesisoccurs in an autoclave at elevated temperature and pressure where a titanium precursor is mixed with water and peptizer (HNO_3). The mixture is then calcined to obtain the nanoparticles[85]. Figure 10 shows the hydrothermal synthesis of titanium dioxide nanorods.

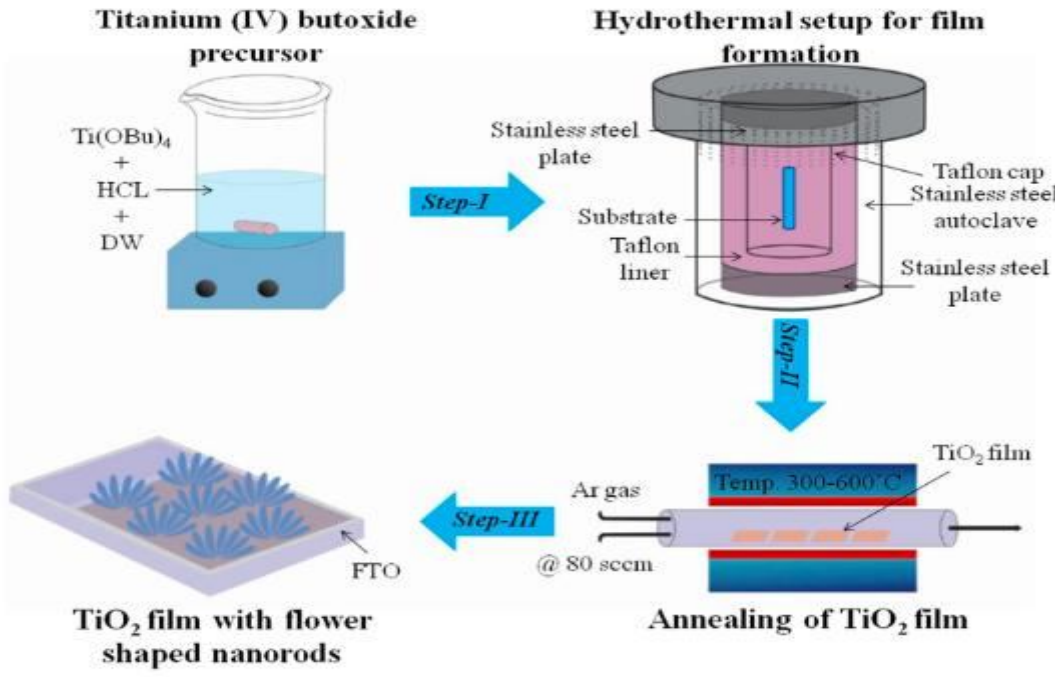

Fig 10. A schematic representation of Titanium dioxide nanorods using hydrothermal synthesis [86].

Sol-gel process usually occurs when an inorganic precursor or metal salt is mixed with water or organic solvent which results in the formation of a sol through hydrolyzing and polymerization. The sol is then transformed into a gel through evaporation which on heating results in generation of nanoparticles[85]. Figure 11 shows the sol gel method for synthesis of TiO_2 nanoparticles.

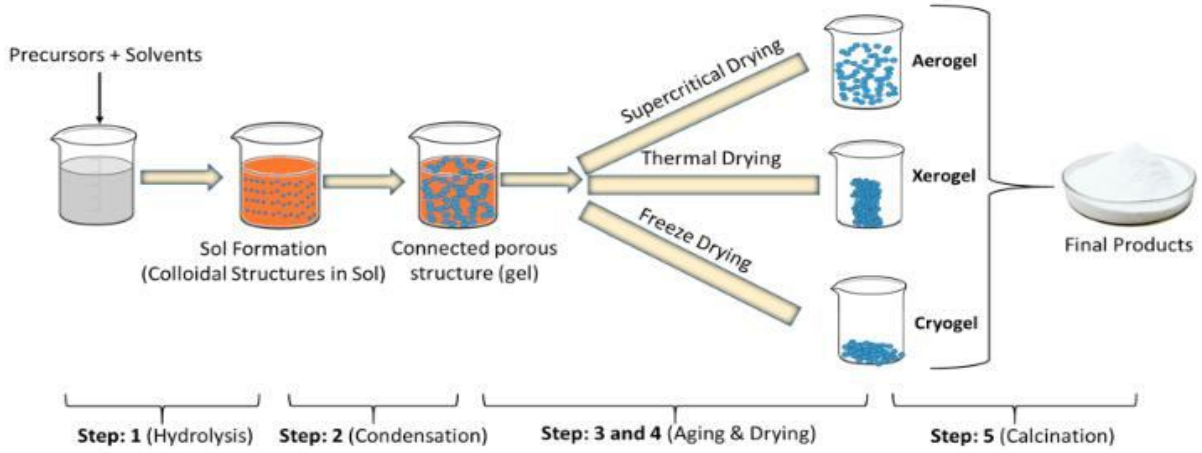

Fig 11. Stepwise formation of nanoparticles using sol-gel synthesis. Reprinted with permission ref [87]. Copyright 2020, Springer

Micelle method normally occurs in the presence of a surfactant as the micelles of TiO_2 precursor are being formed in solution. When temperature changes are applied these micelles form TiO_2 nanoparticles[85].

Related to the hydrothermal process is the solvothermal synthesis however the difference is that during the preparation an organic solvent is mixed with the precursor. For the generation of desired structures, high boiling point solvents are used which are effective at even high temperatures which generate the nanostructures[85]. Figure 12 the solvothermal synthesis technique.

Fig 12. A schematic representation of the solvothermal synthesis. Reprinted with permission ref [88]. Copyright 2023, Springer

Anodization occurs when a potential is applied to TiO_2 metal foil dipped in a fluoride electrolyte solution which results in the formation of the nanotubes. Optimization of the anodization time, pH, electrolyte composition, and potential of the nanotube length can be controlled. Crystalline nanotubes are formed through annealing of amorphous TiO_2 at elevated temperatures[85,89,90].

Flame spray pyrolysis occurs when a titanium precursor is dissolved in water to generate a solution which is then vaporized onto the substrate using a spray nozzle and the process occurs at temperature ranges of (300-500 °C). The spraying of the solvent onto a temperature substrate causes evaporation of the solvent which then results in the formation of nanoparticles[91]. Figure 13 shows flame pyrolysis synthesis technique

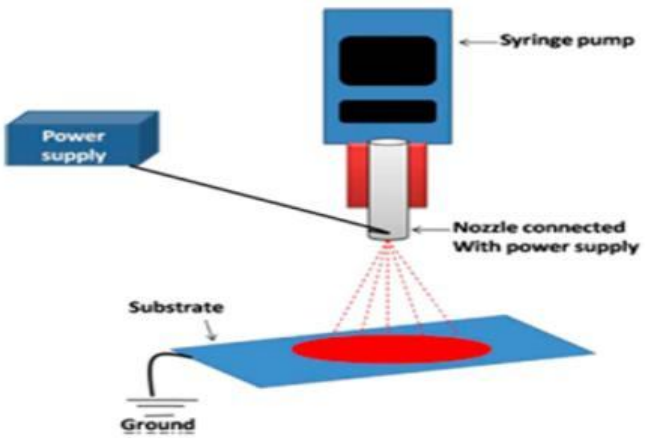

Fig 13. A diagrammatic representation of flame spray pyrolysis [92].

Electrospinning occurs when an electrical charge generates fibers in solution resulting in high aspect ratio nanostructures[93]. Figure 14 shows electrospinning synthesis technique.

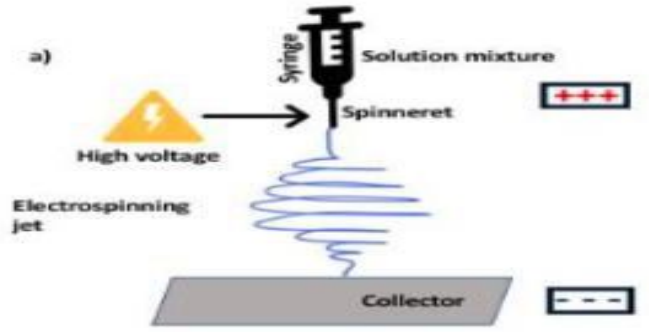

Fig 14. A schematic representation of the electrospinning synthesis [94].

Microwave-assisted generates nanostructures when electromagnetic radiation is used to elevate the temperature of dielectrics[95]. Figure 15 shows micro-wave assisted synthesis of TiO_2 nano powder.

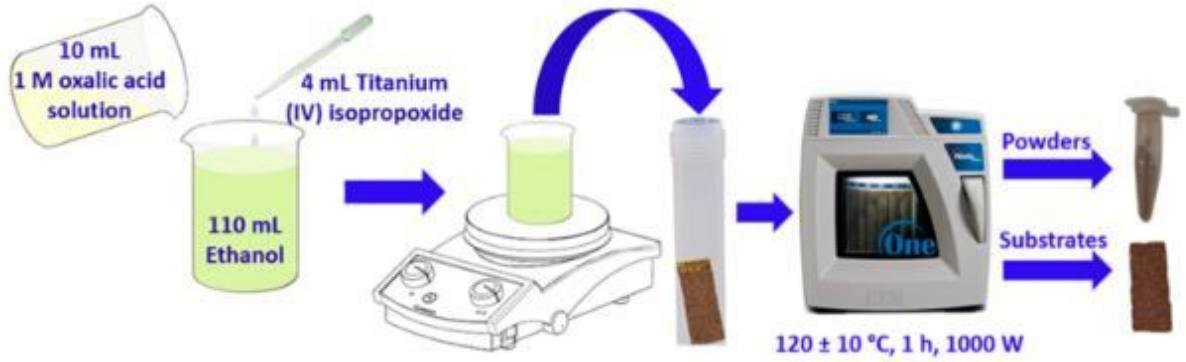

Fig 15. A schematic representation of the microwave-assisted synthesis of TiO_2nano powder[96].

Thermal oxidation occurs through the sputtering or evaporation of a thin TiO_2 film at elevated temperatures in the presence of oxygen for oxidation to happen which generates a TiO_2 compact layer[97].

Direct oxidation is similar to anodization in which it also uses oxidizing agents to generate the preferred nanostructures[98].

Spray pyrolysis resembles flame spray pyrolysis however this method does not generate nanoparticles but instead a dense layer of the TiO_2 precursor is formed on the substrate[99].

Pulsed laser deposition, occurs when a TiO_2 is compressed to form a disk which then acts as a target of the laser. The disk is vaporized by the laser which causes condensation on the substrate resulting in the generation of a thin film[100,101]. Figure 16 shows pulsed laser deposition method.

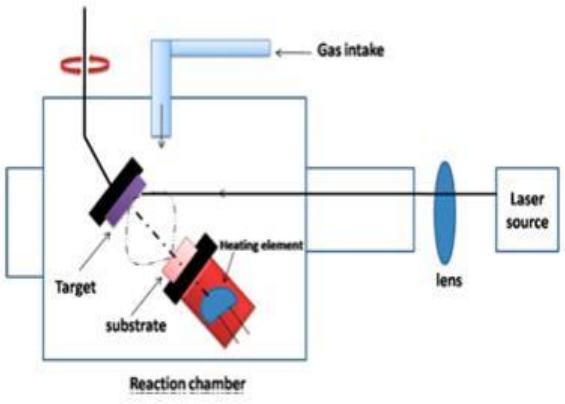

Fig 16. A schematic representation of pulsed laser deposition [92].

Sonochemical synthesis occurs when a solution containing the TiO_2 is ultrasonicated causing intense local heating, enormous cooling rates, and high pressure. This synthesis method generates TiO_2 nanoparticles with a high aspect ratio[85,102].

Spin coating is a technique in which a TiO_2 precursor is spin-coated onto the substrate surface resulting in the formation of a compact layer[103]. Figure 17 shows spin coating synthesis technique.

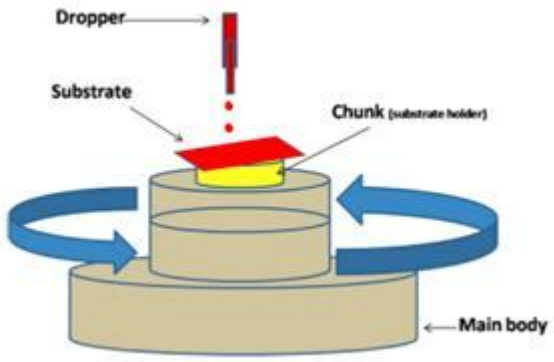

Fig 17. A schematic representation of the spin coating method [92].

Atomic layer deposition occurs when a TiO_2 precursor mixed with water is exposed to a substrate which causes deposition of thick layers on the surface. To control the thickness of the generated layer several cycles are carried out[104]. A schematic process flow diagram of the ALD is shown in Figure 18.

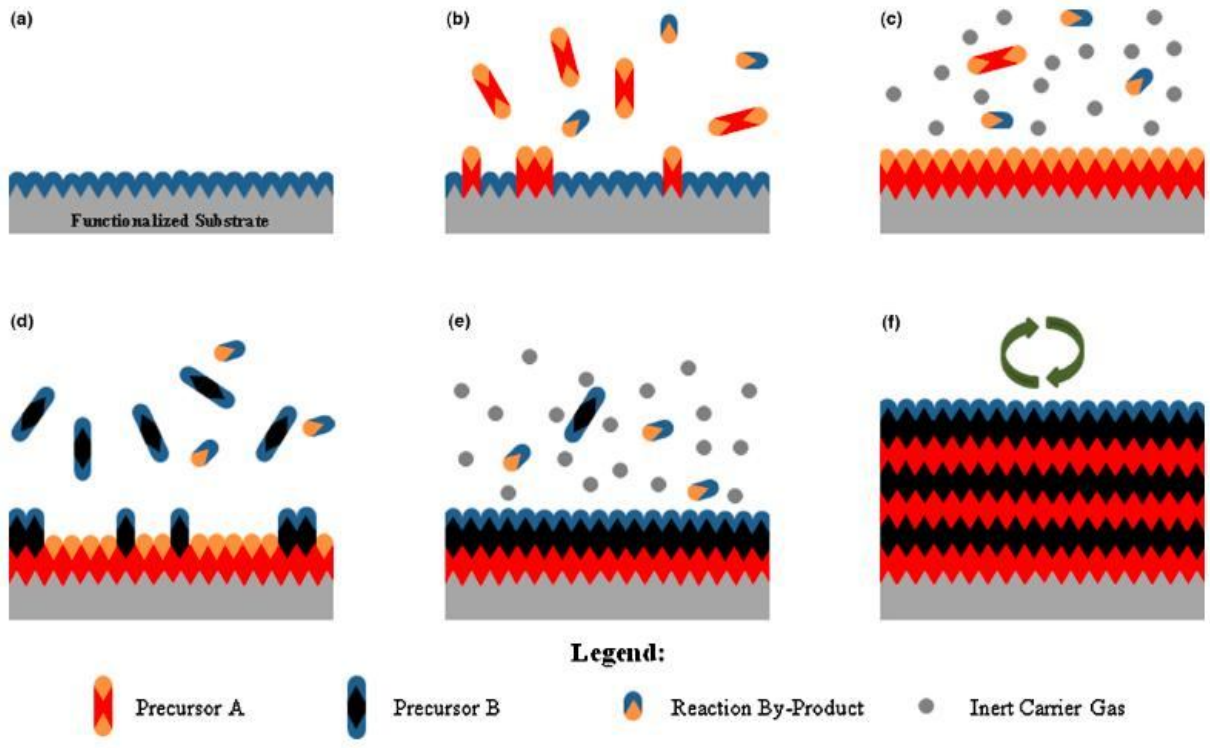

Fig 18. Diagramofatomic layer depositionprocess(a)substratesurfacetreatedtofunctionalizethesurface.(b)PrecursorA ispulsedandreactswiththe surface.(c)Purgingwithinertcarriergas.

(d)PrecursorBispulsedandreactswiththe surface. (e)Purgingwithinertcarriergas. (f)Steps2–5arerepeatedfordesiredthickness[105].

Electrochemical deposition occurs when a TiO_2 precursor is deposited through electrochemical treatment resulting in the formation of a compact layer. When the layer is subjected to heating this generates a crystalline form[106].

4. APPLICATION OF TITANIUM DIOXIDE NANOPARTICLES IN PHOTOCATALYTIC DEGRADATION OF SYNTHETIC DYES

Titanium dioxide nanoparticles have been applied in the degradation of synthetic dyes particularly methylene blue and methyl orange. The photocatalytic activity of TiO_2 is influenced by several factors such as surface area, hydroxyl group density, crystal structure, band gap, and porosity [107]. Doping with non-metals and metals is a simple way of modifying the electronic and structural properties of the nanoparticles as well as reducing on the electron-hole recombination effects.Different metals are used in the modification of Titanium nanoparticles and they include copper, nickel, cobalt, chromium, and manganese. These are known to improve the photocatalytic activity of TiO_2 because of the fast transfer of the photogenerated electron from the conduction band to the noble metal but also reduce the recombination of the holes with the electrons due to improved charge separation[108,109].

4.1 COPPER-DOPED TITANIUM DIOXIDE NANOPARTICLES

Ikram et al [110]synthesized titanium dioxide nanoparticles doped with copper using the sol gel method. Initially, X-ray diffraction analysis was determined and the crystalline phase of anatase was observed with no copper peaks which signifies that all the copper might have formed clustersthat were well incorporated into the surfaces of the nanoparticles Figure 19 (i). It is also noticeable that the dopant peaks have a high intensity due to an increase in the crystallinity as the dopant concentration increases[111]. FTIR spectroscopy showed the presence of Ti-O-Ti within the range of 400-1000 cm-1 which means the presence of TiO_2[112,113] Figure (i). Peaks corresponding to Ti-O-N and O-H are also observed for the synthesized nanoparticles[113]. The hydroxyl group is attributed to the physisorbed water on the nanoparticles during synthesis which is caused by strong Lewis acidity due to the Ti^{4+} coordinately active species[111].HR-TEM was carried out and it showed an ordered arrangement of the nanoparticles which form

single layers at particular areas Figure (ii). The arrangement is well in agreement with x-ray diffraction analysis as seen from (101) facet plane of the anatase phase. Ultraviolet visible spectroscopy was carried out to determine the optical transition mainly caused by the transition of electrons from the valence to the conduction band which gives information about the absorption range Figure (iii). Pure TiO_2 shows an absorbance around 310 nm which is also depicted by copper-doped TiO_2 which further moves towards the visible spectral range. The increase in wavelength is caused by electronic transitions from O 2p to Cu 3d states, another band is observed around 500-700 nm which is ascribed to d-d transition in the 3d9 electronic configuration of copper[114–116]. In addition, PL studies were carried out and they showed TiO_2 surface defects and oxygen vacancies at a peak position of 431 nm. It is noted that with an increase in dopant concentration, the intensity of the PL peak decreases which leads to a reduction in recombination effects but also an improvement in the separation efficiency. PL intense peak at 431 nm is caused by luminescence centers whose purpose is to enhance the photostability of TiO_2[117]. Figure 19 (iii) shows the photocatalytic degradation of methylene blue in the presence of pure and doped TiO_2 nanoparticles. It is observed that the degradation increases as the dopant concentration increases due to the creation of an intermediate energy gap but also in the reduction of recombination. Isotherm and kinetic studies of the nanoparticles on methylene blue degradation were observed [118]. In the presence of visible light, the highest degradation was observed to be 99 % for (0.09:1) of Cr: TiO_2 nanoparticles. Pure TiO_2 caused a photocatalytic degradation of 40 % when the light was turned on.

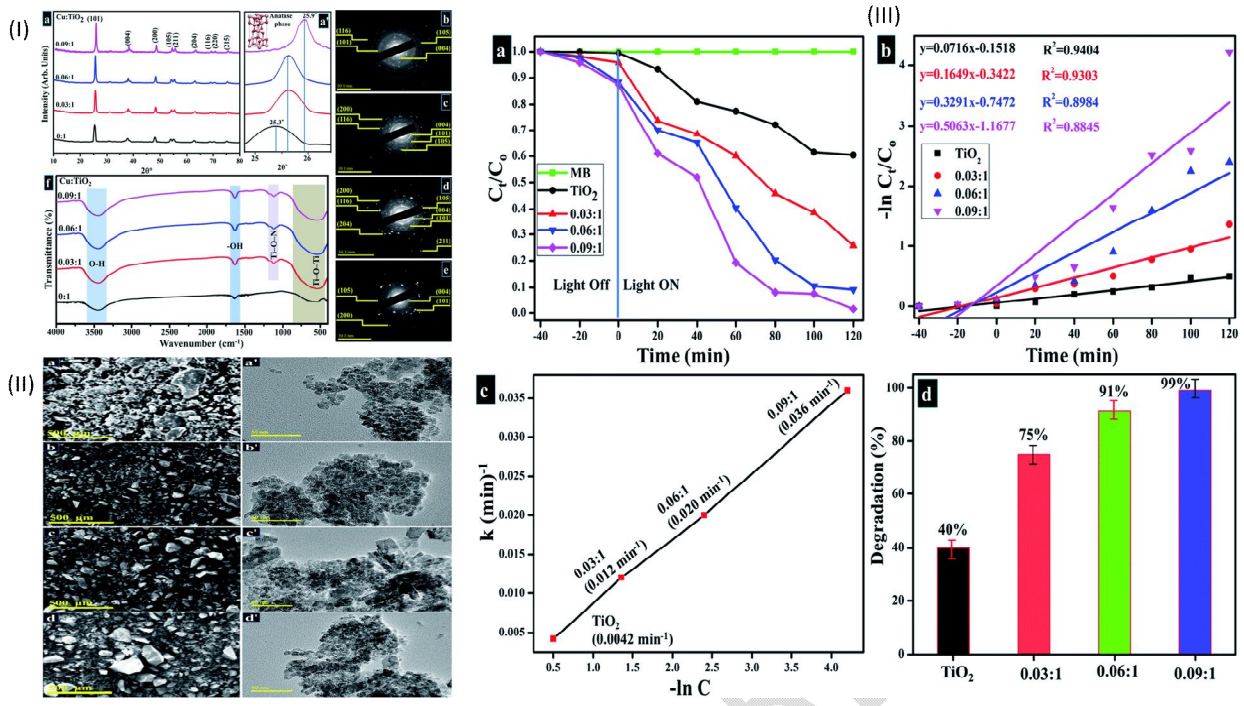

Fig 19. (i) X-ray diffraction and Fourier transform infrared spectroscopy peaks, (ii) HR-TEM, (iii)kinetics, isotherm, and photocatalytic plots of the synthesized copper doped titanium dioxide nanoparticles.

4.2 NICKEL-DOPED TITANIUM DIOXIDE NANOPARTICLES

Guan et al [119] developed Nickel doped Titanium dioxide nanoparticles for the photodegradation of methylene blue dye. The doped nanoparticles were initially characterized before they were added to the solution. X-ray diffraction in Figure 20 (i) shows thatthe Ni–TiO_2 sample exhibits peaks at 25.28°, 37.80°, 48.05°, 53.89°, 55.06°, 62.69°, 70.31°, and 75.03°, corresponding to the anatase phase (JCPDF 21-1272), with no other phases. The spectra do not show any Nickel peaks as such indicating that the dopant was successfully incorporated into the crystal lattice of TiO_2[120]. The scanning electron microscopy image in Figure 20 (i) showed spherically images of the doped nanoparticles which are homogeneous with a size range of 20-30 nm. Using UV as shown in Figure 20 (ii) the Ni-TiO_2 nanoparticles have a particularly broader absorption (visible spectrum) as compared to undoped as such degrade further confirming that doping improves on the photocatalytic activity. Figure 20 (iii) shows the photodegradation of methylene blue in the presence of solar and UV radiation for both doped and undoped TiO_2. It is observed that the photocatalytic activity of Ni-TiO_2 was superior with

efficiencies of 92.7 and 96.3 % for UV and solar radiation respectively compared to 85.9 and 27.7 % for pure TiO_2. In addition, the nitrogen desorption isotherm in Figure 20 (iv) confirms that the doped TiO_2 has a mesoporous surface which can further cause the adsorption of small dyes onto the photocatalyst surface[121].

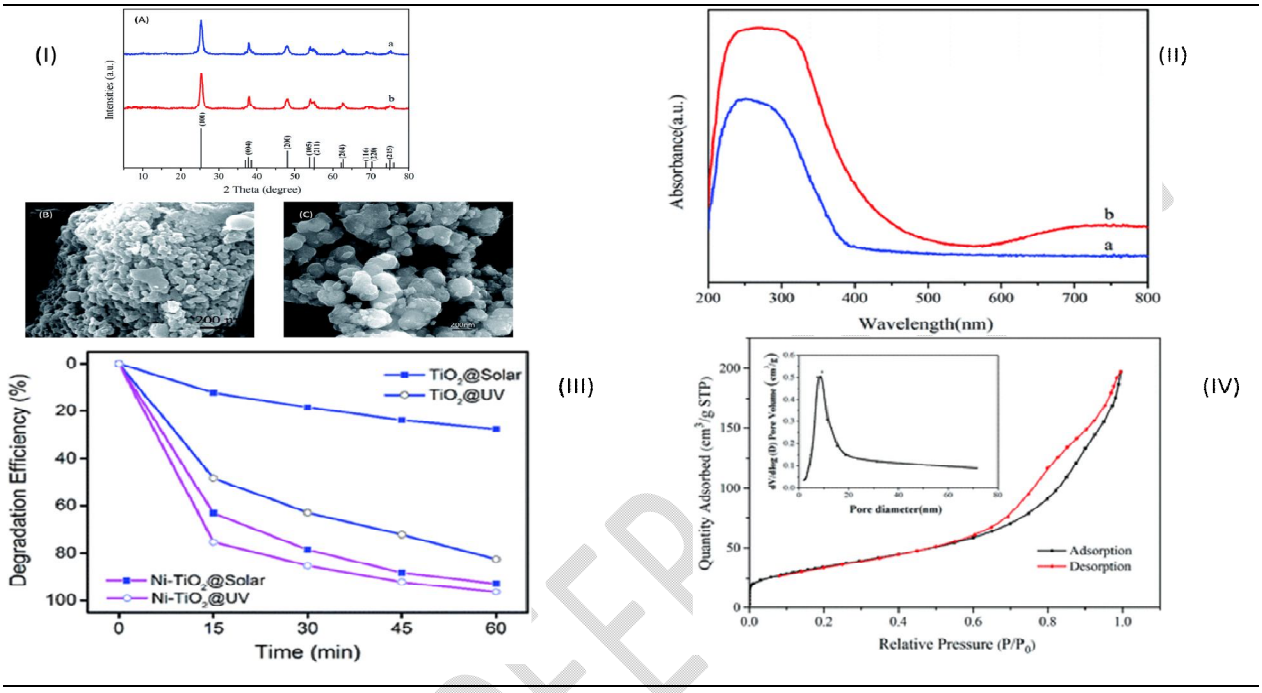

Fig 20. (i) X-ray diffraction and scanning electron microscopy, (ii) Ultraviolet-visible spectra of pure and doped TiO_2 nanoparticles, (iii) nitrogen adsorption-desorption isotherm, (iv) UV photocatalytic degradation methylene blue of Nickel doped titanium doped nanoparticles.

4.3 COBALT-DOPED TITANIUM DIOXIDE NANOPARTICLES

Mragui et al [122] synthesized cobalt-doped titanium dioxide nanoparticles using the sol gel and precipitation method. The X-ray diffraction in Figure 21 (i) shows peaks of pure anatase form as observed. It is observed that the peaks of TiO_2 decrease as the concentration of cobalt is increased (10%) which gives an insight that the nanoparticles have undergone some transformation[123–125]. From this analysis,it is observed that the only peaks present as those of pure TiO_2 and as such indicating that cobalt was well incorporated into the crystal lattice of the nanoparticles. Figure 21 (ii) shows the scanning electron microscopy image of the TiO_2 has agglomerated nanoparticles with irregular and spherical shapes which increase as the concentration of cobalt increases[126]. In addition, UV-vis as shown in Figure 21 (iii) was

carried out on the sample and it was observed that TiO_2 had an absorbance below 350 nm which decreases as the wavelength tends to the visible range. Doped TiO_2 has an increase in absorbance as the concentration of cobalt (1 – 10 %) increases which is an indication that the photocatalytic activity of the nanoparticles increases. The Tauc's plot insert also demonstrates that with 1 and 10 % cobalt concentration the band gap reduces to 3.05 and 2.94 eV respectively. Furthermore, photoluminescence spectroscopy in Figure 21 (iv) which analyzes the electronic structure, transfer behavior, and recombination effects of the electrons and holes demonstrated a reduction as doping with cobalt was increased. It is worth mentioning that the PL intensity correlates with electron/hole recombination effects and it shows a strong intensity peak at 357 nm which relatesto pure TiO_2[127]. Lower intensity PL peaks signify a decrease in the recombination effects thus a high photocatalytic activity. Lastly, the photodegradation of methyl orange dye was studied and it was observed that 1 % cobalt-doped TiO_2 had the best photocatalytic activity and this is also in agreement with the characterization techniques as shown in Figure 21 (v). Previous studies have determined that an increase in the metal concentration results in recombination which leads to a reduction in photocatalytic activity[128–130].

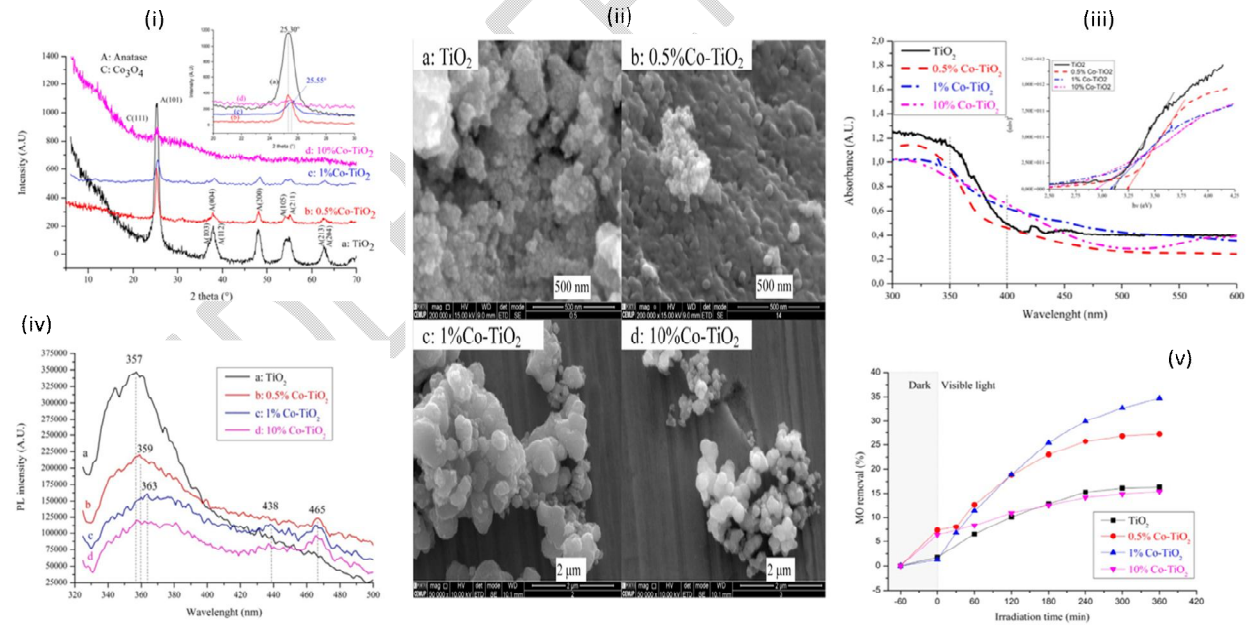

Fig 21. (i) X-ray diffraction, (ii) scanning electron microscopy, (iii) Ultraviolet spectra of doped and pure TiO_2, (iv) X-ray photoelectron spectra, (v) photocatalytic degradation of methyl orange dye of doped and pure TiO_2.

4.4 CHROMIUM-DOPED TITANIUM DIOXIDE NANOPARTICLES

Abushad et al [131]synthesized chromium-doped TiO_2 nanoparticles using the sol gel method. Transmission electron microscopyimageofundoped TiO_2 exhibits elongated nanoparticles with a size range of 4 to 20 nm. Figure (ii) of TEM further showed that chromium-doped TiO_2 nanoparticles had large particles and this was confirmed using the single distribution histogram.Figure 22 (i) and (ii) using selected area electron diffraction (SAED) revealed the bright spotty ring patterns which are responsible for the polycrystalline nature. Figure 22 (iii) shows the X-ray photoelectron spectra (XPS) doped and undoped TiO_2 reveals the existence of the different elements that is TiO_2, Cr, O, and C and it further demonstrates prominent peaks of C 1s, O 1s, and Ti 2p. The Ti 2p peaks are consistent with Ti^{4+} valence oxidation state and then the observed decrease in intensity is attributed to an increase in chromium doping due to a reduction in the formation of a mixed oxide of titania. In figure 22 (iv) FESEM micrographs of both doped and undoped TiO_2 show that agglomeration occurs in undoped TiO_2 compared to 5 % doped TiO_2 which is attributed to the magnetic interaction of the nanoparticles. Raman spectrashow five active modes which correspond to TiO_2 while the sixth mode at 392 is assigned to undoped and doped nanoparticles[132,133] as shown in Figure 22 (v). In addition to the Raman spectra, the insert figure shows a displacement in the wavelength as the concentration of chromium increases which then decreases above 10 % due to lattice contraction thus causing a blue shift[134].Figure 22 (vi A) shows the UV spectra of methylene blue before the addition of the photocatalyst. Figure (vi B) shows the changes in methylene blue concentration for every interval of 5 mins (5 – 40 mins) in the presence of pure TiO_2 and chromium-doped TiO_2. Figure (vi C) shows the percentage of the methylene blue degraded by both pure and chromium-doped TiO_2 and it is observed that 20 % chromium had the highest percentage (89.86 %).

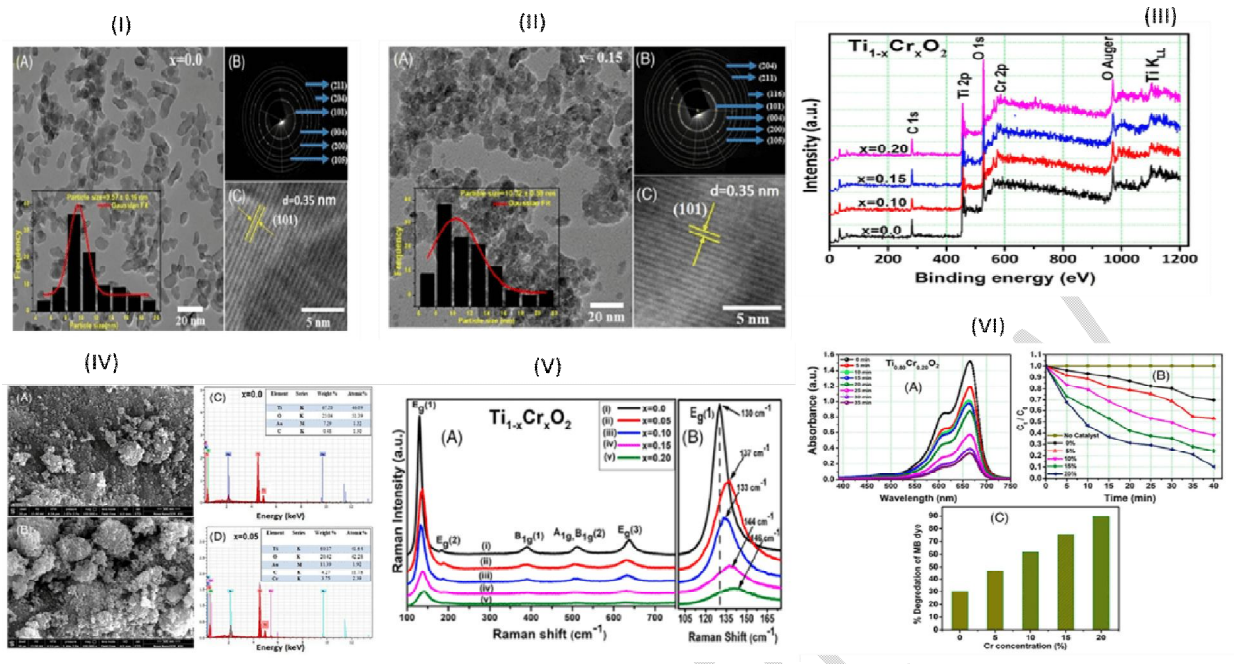

Fig 22. (i) TEM, (ii) SAED images, (iii) X-ray photoelectron spectra, (iv) Field emission scanning electron microscopy, (v) Raman spectroscopy, (vi) UV absorbance peaks, changes in methylene blue concentration and removal efficiency studies of synthesized chromium doped titanium dioxide nanoparticles.

4.5 MANGANESE-DOPED TITANIUM DIOXIDE NANOPARTICLES

Deng et al [135]synthesized manganese-doped TiO_2 nanoparticles using the sol-gel technique. Initially, X-ray diffraction was carried it was observed that the peaks of pure and doped phases are due to the anatase nature of TiO_2 as shown in Figure 23 (i). It is seen that the peak width of the anatase form broadens as the concentration of manganese is increased but also the manganese oxide peaks are not observed even at concentrations of 12 %.In addition, XPS was carried out and it was observed that Ti 2p had two spin-orbit doublet peaks at Ti $2P_{3/2}$ and Ti $2P_{1/2}$ which corresponds tothe Ti^{4+} valence oxidation state. Figure 23 (ii) shows the XPS peaks of 2 % and 12 % manganese concentration which shows multiple peaks in which the major represents an oxidation state of Mn^{3+} while the minor peak with higher binding energy is due to a higher oxidation state preferably Mn^{4+}. Figure 23 (iii) shows the UV spectra of pure and doped TiO_2 nanoparticles. Pure TiO_2 shows a typical sharp edge at 400 nm due to the excitation of electrons from the valence to the conduction band of the semiconductor. It is also observed that the

manganese doped nanoparticles have a second absorbance peak which is in the visible spectral region when the concentration is increased to 12 % the infrared region of the spectra is also occupied. This is consistent with previous studies in which this causes a red shift which causes a reduction in the band gap due to the introduction of curvy intermediates into the forbidden band gap[136]. Figure 23 (iv) shows TEM analysis and it is observed that both doped and pure TiO_2 have uniform nanocrystalline structure which is consistent with x-ray diffraction.Furthermore (SEAD) was determined and it was observed that dark polycrystalline rings are due to the anatase form of TiO_2 and no phases are observed due to either formation of oxides on the surface. Figure 23 (v) shows that visible light photocatalytic degradation of methylene blue was studied using both doped and undoped TiO_2. The undoped nanoparticles show a slight degradation of methylene blue due to their low absorption in the visible range. Titanium dioxide nanoparticles doped with 0.2 % manganese had the highest photocatalytic activity due to a narrower band gap, and the incorporation of manganese into the crystal lattice of TiO_2 which generates intermediate bands but also the small grain particles which account for the large surface area hence facilitate degradation[137]. It is worth mentioning from previous studies that a high concentration affects the photocatalytic activity due to the creation of crystal defects that act as recombination centers[137].

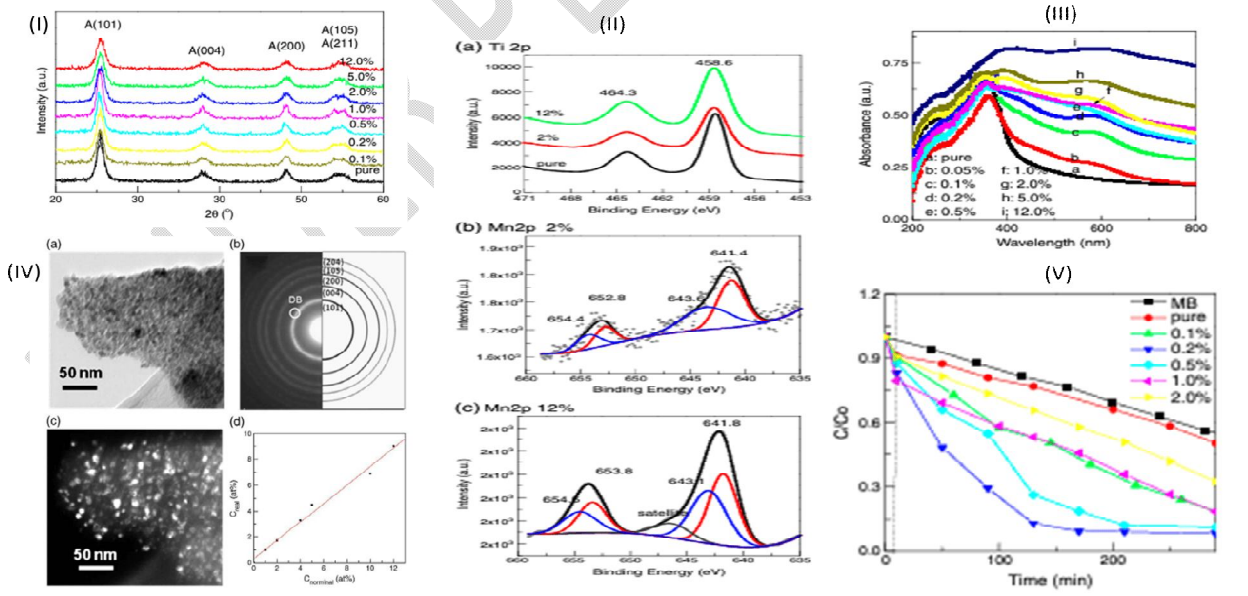

Fig 23. (i) X-ray diffraction, (ii) X-ray photoelectron spectra, (iii) Ultraviolet spectra of doped and undoped TiO2, (iv) TEM and SAED, and (v) photocatalytic degradation of methylene blue of the synthesized nanoparticles.

5. CONCLUSION

Titanium dioxide nanoparticles are used in the photocatalytic degradation of synthetic dyes into water and carbon dioxide which are less toxic by-products. Synthetic dyes are classified into ionic and non-ionic dyes which can further be grouped into vat, disperse, acid, direct, and reactive dyes. The nanoparticles have low photocatalytic activity during the degradation process due to a wide band gap which favors electron-hole recombination effects. Doping with transition metals such as chromium, cobalt, nickel, copper and manganese is an alternative way of improving the band gap to lower than 3.0 eV which reduces the recombination effects and improves the structural and electronic properties. Synthesis of doped titanium dioxide nanoparticles is through a variety of techniques such as chemical vapor deposition, sol gel method, sonochemical synthesis, spray pyrolysis, etc. The sol gel method is used as an alternative method since it generates crystalline particles with large surface area and gives off no by-products. Characterization techniques such as Transmission electron microscopy, scanning electron microscopy, x-ray diffraction, ultra-violet visible spectroscopy, and nitrogen desorption-adsorption isotherms are used to analyze the doped nanoparticles and photocatalytic activity.

Disclaimer (Artificial intelligence)

Author(s) hereby declare that NO generative AI technologies such as Large Language Models (ChatGPT, COPILOT, etc) and text-to-image generators have been used during writing or editing of manuscripts.

Reference

1. Bbumba S, Karume I, Kigozi M, Oyege I, Ntale M. How Components of Dye-sensitized Solar Cells Contribute to Efficient Solar Energy Capture. Asian Journal of Applied Chemistry Research. 2024;15(2):24–40.

2. Saeed M, Usman M, Ibrahim M, Haq A ul, Khan I, Ijaz H, et al. Enhanced photo catalytic degradation of methyl orange using p–n Co3O4-TiO2 hetero-junction as catalyst. 2020;18(5–6). Available from: https://doi.org/10.1515/ijcre-2020-0004

3. Zeghioud H, Khellaf N, Amrane A, Djelal H, Bouhelassa M, Assadi AA, et al. Combining photocatalytic process and biological treatment for Reactive Green 12 degradation: optimization, mineralization, and phytotoxicity with seed germination. Environmental Science and Pollution Research [Internet]. 2021;28(10):12490–9. Available from: https://doi.org/10.1007/s11356-020-11282-1

4. Muneer M, Hafiz N, Usman M, Rehman FU, Saeed M, Bhatti H, et al. Environmentally friendly oxidative degradation of reactive orange dye by high energy radiation. Oxid Commun. 2015;38(4):2091.

5. Karume I, Bbumba S, Kigozi M, Nabatanzi A, Mukasa I harq ZT, Yiga S. One-pot removal of pharmaceuticals and toxic heavy metals from water using xerogel-immobilized quartz/banana peels-activated carbon. Green Chem Lett Rev. 2023;16(1):2238726.

6. Abdi J, Vossoughi M, Mahmoodi NM, Alemzadeh I. Synthesis of metal-organic framework hybrid nanocomposites based on GO and CNT with high adsorption capacity for dye removal. Chemical Engineering Journal. 2017 Oct 15;326:1145–58.

7. Li Y, Zhou Y, Zhou Y, Lei J, Pu S. Cyclodextrin modified filter paper for removal of cationic dyes/Cu ions from aqueous solutions. Water Science and Technology. 2018;78(12):2553–63.

8. He W, Li N, Wang X, Hu T, Bu X. A cationic metal-organic framework based on {Zn4} cluster for rapid and selective adsorption of dyes. Chinese Chemical Letters. 2018;29(6):857–60.

9. Eghbali P, Hassani A, Sündü B, Metin Ö. Strontium titanate nanocubes assembled on mesoporous graphitic carbon nitride (SrTiO3/mpg-C3N4): preparation, characterization and catalytic performance. J Mol Liq. 2019;290:111208.

10. Zhou Y, Lu J, Zhou Y, Liu Y. Recent advances for dyes removal using novel adsorbents: a review. Environmental pollution. 2019;252:352–65.

11. Program NT. Toxicology and carcinogenesis studies of methylene blue trihydrate (Cas No. 7220-79-3) in F344/N rats and B6C3F1 mice (gavage studies). Natl Toxicol Program Tech Rep Ser. 2008;(540):1–224.

12. Khan S, Noor T, Iqbal N, Yaqoob L. Photocatalytic Dye Degradation from Textile Wastewater: A Review. ACS Omega. 2024;

13. Idris MO, Ibrahim MNM, Noh NAM, Yaqoob AA, Daud NNM, Hussin MH, et al. Assessment of biomass material as valuable electrode for high energy performance in microbial fuel cell with biodegradation of organic pollutant. Fuel. 2024;371:132059.

14. Emmanuel SS, Adesibikan AA, Saliu OD, Opatola EA. Greenly biosynthesized bimetallic nanoparticles for ecofriendly degradation of notorious dye pollutants: A review. Plant Nano Biology. 2023;3:100024.

15. Katheresan V, Kansedo J, Lau SY. Efficiency of various recent wastewater dye removal methods: A review. J Environ Chem Eng. 2018;6(4):4676–97.

16. Demirkıran N, Özdemir GDT, Saraç M, Dardağan M. Adsorption of methylene blue from aqueous solutions by pyrolusite ore. Mongolian Journal of Chemistry. 2017;18(44):5–11.

17. Idris MO, Yaqoob AA, Ibrahim MNM, Ahmad A, Alshammari MB. Introduction of adsorption techniques for heavy metals remediation. In: Emerging Techniques for Treatment of Toxic Metals from Wastewater. Elsevier; 2023. p. 1–18.

18. Comninellis C, Kapalka A, Malato S, Parsons SA, Poulios I, Mantzavinos D. Advanced oxidation processes for water treatment: advances and trends for R&D. Journal of Chemical Technology & Biotechnology: International Research in Process, Environmental & Clean Technology. 2008;83(6):769–76.

19. Deng Y, Zhao R. Advanced Oxidation Processes (AOPs) in Wastewater Treatment. Curr Pollut Rep [Internet]. 2015;1(3):167–76. Available from: https://doi.org/10.1007/s40726-015-0015-z

20. Ghanbari F, Moradi M. Application of peroxymonosulfate and its activation methods for degradation of environmental organic pollutants: Review. Chemical Engineering Journal. 2017 Feb 15;310:41–62.

21. Ibrahim SM, Badawy AA, Essawy HA. Improvement of dyes removal from aqueous solution by Nanosized cobalt ferrite treated with humic acid during coprecipitation. J Nanostructure Chem [Internet]. 2019;9(4):281–98. Available from: https://doi.org/10.1007/s40097-019-00318-9

22. Tomar R, Abdala AA, Chaudhary RG, Singh NB. Photocatalytic degradation of dyes by nanomaterials. Mater Today Proc. 2020 Jan 1;29:967–73.

23. Zhang T, Liu Y, Zhong S, Zhang L. AOPs-based remediation of petroleum hydrocarbons-contaminated soils: Efficiency, influencing factors and environmental impacts. Chemosphere. 2020 May 1;246:125726.

24. Sgroi M, Snyder SA, Roccaro P. Comparison of AOPs at pilot scale: Energy costs for micro-pollutants oxidation, disinfection by-products formation and pathogens inactivation. Chemosphere. 2021 Jun 1;273:128527.

25. Miklos DB, Wang WL, Linden KG, Drewes JE, Hübner U. Comparison of UV-AOPs (UV/H2O2, UV/PDS and UV/Chlorine) for TOrC removal from municipal wastewater effluent and optical surrogate model evaluation. Chemical Engineering Journal. 2019 Apr 15;362:537–47.

26. Amor C, Rodríguez-Chueca J, Fernandes JL, Domínguez JR, Lucas MS, Peres JA. Winery wastewater treatment by sulphate radical based-advanced oxidation processes (SR-AOP): Thermally vs UV-assisted persulphate activation. Process Safety and Environmental Protection. 2019 Feb 1;122:94–101.

27. Wang J, Zhuan R. Degradation of antibiotics by advanced oxidation processes: An overview. Science of The Total Environment. 2020 Jan 20;701:135023.

28. Mazivila SJ, Ricardo IA, Leitão JMM, Esteves da Silva JCG. A review on advanced oxidation processes: From classical to new perspectives coupled to two- and multi-way calibration strategies to monitor degradation of contaminants in environmental samples. Trends in Environmental Analytical Chemistry. 2019 Oct 1;24:e00072.

29. Reza KM, Kurny ASW, Gulshan F. Parameters affecting the photocatalytic degradation of dyes using TiO2: a review. Appl Water Sci [Internet]. 2017;7(4):1569–78. Available from: https://doi.org/10.1007/s13201-015-0367-y

30. Kim S, Hwang SJ, Choi W. Visible light active platinum-ion-doped TiO2 photocatalyst. J Phys Chem B. 2005;109(51):24260–7.

31. Al-Harbi LM, Kosa SA, Abd El Maksod IH, Hegazy EZ. The Photocatalytic Activity of TiO2□Zeolite Composite for Degradation of Dye Using Synthetic UV and Jeddah Sunlight. J Nanomater. 2015;2015(1):565849.

32. Hassan ME, Chen J, Liu G, Zhu D, Cai J. Enhanced photocatalytic degradation of methyl orange dye under the daylight irradiation over CN-TiO2 modified with OMS-2. Materials. 2014;7(12):8024–36.

33. Malato S, Blanco J, Campos A, Cáceres J, Guillard C, Herrmann JM, et al. Effect of operating parameters on the testing of new industrial titania catalysts at solar pilot plant scale. Appl Catal B. 2003;42(4):349–57.

34. Chatterjee D, Dasgupta S. Visible light induced photocatalytic degradation of organic pollutants. Journal of Photochemistry and Photobiology C: Photochemistry Reviews. 2005;6(2–3):186–205.

35. Aramendía MA, Marinas A, Marinas JM, Moreno JM, Urbano FJ. Photocatalytic degradation of herbicide fluroxypyr in aqueous suspension of TiO2. Catal Today. 2005;101(3–4):187–93.

36. Bbumba S, Karume I, Kigozi M, Nsamba HK, Yikii CL, Nazziwa RA, et al. Titanium Dioxide One-Dimensional Nanostructures as Photoanodes for Dye-Sensitized Solar Cells. Journal of Materials Science Research and Reviews. 2024;7(2):315–38.

37. Singh MK, Mehata MS. Enhanced photoinduced catalytic activity of transition metal ions incorporated TiO2 nanoparticles for degradation of organic dye: Absorption and photoluminescence spectroscopy. Opt Mater (Amst). 2020 Nov 1;109:110309.

38. Pei L, Luo Y, Saleem MA, Wang J. Sustainable pilot scale reactive dyeing based on silicone oil for improving dye fixation and reducing discharges. J Clean Prod. 2021 Jan 10;279:123831.

39. Anliker R. Colour chemistry and the environment. Review of Progress in Coloration and Related Topics. 1977;8(1):60–72.

40. Srinivasan A, Viraraghavan T. Decolorization of dye wastewaters by biosorbents: A review. J Environ Manage. 2010 Oct 1;91(10):1915–29.

41. Afatt SS, Mahdi HA. Synthesis and Characterization of a new Schiff Base {N-(2-{[(4-bromophenyl) imino] methyl} phenyl) acetamide} and its complexes with some transition metal. Journal of College of Education for Pure Science. 2012;2(4):110–7.

42. Gürses A, Açıkyıldız M, Güneş K, Gürses MS. Dyes and Pigments: Their Structure and Properties. In: Gürses A, Açıkyıldız M, Güneş K, Gürses MS, editors. Dyes and Pigments [Internet]. Cham: Springer International Publishing; 2016. p. 13–29. Available from: https://doi.org/10.1007/978-3-319-33892-7_2

43. Benaissa A. Etude de la faisabilité d'élimination de certains colorants textiles par certains matériaux déchets d'origine naturelle. 2012;

44. Berradi M, Hsissou R, Khudhair M, Assouag M, Cherkaoui O, El Bachiri A, et al. Textile finishing dyes and their impact on aquatic environs. Heliyon. 2019;5(11).

45. Miladinova PM, Vaseva RK, Lukanova VR. On the synthesis and application of some mono-and dis-azo acid dyes. J Chem Technol Metall. 2016;51(3):249–56.

46. Gupta VK, Suhas. Application of low-cost adsorbents for dye removal – A review. J Environ Manage. 2009 Jun 1;90(8):2313–42.

47. Wu J, Li Q, Li W, Li Y, Wang G, Li A, et al. Efficient removal of acid dyes using permanent magnetic resin and its preliminary investigation for advanced treatment of dyeing effluents. J Clean Prod. 2020 Apr 1;251:119694.

48. Khatri A, Peerzada MH, Mohsin M, White M. A review on developments in dyeing cotton fabrics with reactive dyes for reducing effluent pollution. J Clean Prod. 2015 Jan 15;87(1):50–7.

49. Cai Y, Liang Y, Navik R, Zhu W, Zhang C, Pervez MN, et al. Improved reactive dye fixation on ramie fiber in liquid ammonia and optimization of fixation parameters using the Taguchi approach. Dyes and Pigments. 2020 Dec 1;183:108734.

50. Siddiqua UH, Irfan M, Ali S, Sahar A, Khalid M, Mahr MS, et al. Computational and experimental study of heterofunctional azo reactive dyes synthesized for cellulosic fabric. J Mol Struct. 2020 Dec 5;1221:128753.

51. Shen C, Pan Y, Wu D, Liu Y, Ma C, Li F, et al. A crosslinking-induced precipitation process for the simultaneous removal of poly(vinyl alcohol) and reactive dye: The

importance of covalent bond forming and magnesium coagulation. Chemical Engineering Journal. 2019 Oct 15;374:904–13.

52. Garg D, Majumder CB, Kumar S, Sarkar B. Removal of Direct Blue-86 dye from aqueous solution using alginate encapsulated activated carbon (PnsAC-alginate) prepared from waste peanut shell. J Environ Chem Eng. 2019 Oct 1;7(5):103365.

53. Lorimer JP, Mason TJ, Plattes M, Phull SS, Walton DJ. Degradation of dye effluent. Pure and Applied Chemistry. 2001;73(12):1957–68.

54. Sharma J, Sharma S, Soni V. Classification and impact of synthetic textile dyes on Aquatic Flora: A review. Reg Stud Mar Sci. 2021 Jun 1;45:101802.

55. Burkinshaw SM, Son YA. The dyeing of supermicrofibre nylon with acid and vat dyes. Dyes and Pigments. 2010 Oct 1;87(2):132–8.

56. Khatri M, Ahmed F, Shaikh I, Phan DN, Khan Q, Khatri Z, et al. Dyeing and characterization of regenerated cellulose nanofibers with vat dyes. Carbohydr Polym. 2017 Oct 15;174:443–9.

57. Kulandainathan MA, Muthukumaran A, Patil K, Chavan RB. Potentiostatic studies on indirect electrochemical reduction of vat dyes. Dyes and Pigments. 2007 Jan 1;73(1):47–54.

58. Considine DM, Considine GD. Van Nostrand's scientific encyclopedia. Springer Science & Business Media; 2013.

59. Clark M. Fundamental principles of dyeing. Handbook of textile and industrial dyeing: Principles, processes and types of dyes. 2011;1:3–27.

60. Zhou X, Zhou Y, Liu J, Song S, Sun J, Zhu G, et al. Study on the pollution characteristics and emission factors of PCDD/Fs from disperse dye production in China. Chemosphere. 2019 Aug 1;228:328–34.

61. Qiu J, Tang B, Ju B, Zhang S, Jin X. Clean synthesis of disperse azo dyes based on peculiar stable 2,6-dibromo-4-nitrophenyl diazonium sulfate. Dyes and Pigments. 2020 Feb 1;173:107920.

62. Asif Tahir M, Bhatti HN, Iqbal M. Solar Red and Brittle Blue direct dyes adsorption onto Eucalyptus angophoroides bark: Equilibrium, kinetics and thermodynamic studies. J Environ Chem Eng. 2016 Jun 1;4(2):2431–9.

63. Gangopadhyay S, Bok S. Evaluation of hybrid sol-gel incorporated with nanoparticles as nano paint. In: AIP Conference Proceedings. 2016.

64. Chen H, Nanayakkara CE, Grassian VH. Titanium dioxide photocatalysis in atmospheric chemistry. Chem Rev. 2012;112(11):5919–48.

65. Haider AJ, Jameel ZN, Al-Hussaini IHM. Review on: titanium dioxide applications. Energy Procedia. 2019;157:17–29.

66. Samat MH, Ali AMM, Taib MFM, Hassan OH, Yahya MZA. Hubbard U calculations on optical properties of 3d transition metal oxide TiO2. Results Phys. 2016;6:891–6.

67. Fang WQ, Gong XQ, Yang HG. On the unusual properties of anatase TiO2 exposed by highly reactive facets. J Phys Chem Lett. 2011;2(7):725–34.

68. Augustynski J. The role of the surface intermediates in the photoelectrochemical behaviour of anatase and rutile TiO2. Electrochim Acta. 1993;38(1):43–6.

69. Sun J, Gao L, Zhang Q. Synthesizing and comparing the photocatalytic properties of high surface area rutile and anatase titania nanoparticles. Journal of the American Ceramic Society. 2003;86(10):1677–82.

70. Deng X, Yue Y, Gao Z. Gas-phase photo-oxidation of organic compounds over nanosized TiO2 photocatalysts by various preparations. Appl Catal B. 2002;39(2):135–47.

71. Ohno T, Sarukawa K, Matsumura M. Crystal faces of rutile and anatase TiO 2 particles and their roles in photocatalytic reactions. New journal of chemistry. 2002;26(9):1167–70.

72. Kasanen J, Suvanto M, Pakkanen TT. Self□cleaning, titanium dioxide based, multilayer coating fabricated on polymer and glass surfaces. J Appl Polym Sci. 2009;111(5):2597–606.

73. Zhang XT, Sato O, Taguchi M, Einaga Y, Murakami T, Fujishima A. Self-cleaning particle coating with antireflection properties. Chemistry of Materials. 2005;17(3):696–700.

74. Birkefeld LD, Azad AM, Akbar SA. Carbon monoxide and hydrogen detection by anatase modification of titanium dioxide. Journal of the American Ceramic Society. 1992;75(11):2964–8.

75. Dutta PK, Ginwalla A, Hogg B, Patton BR, Chwieroth B, Liang Z, et al. Interaction of carbon monoxide with anatase surfaces at high temperatures: optimization of a carbon monoxide sensor. J Phys Chem B. 1999;103(21):4412–22.

76. O'regan B, Grätzel M. A low-cost, high-efficiency solar cell based on dye-sensitized colloidal TiO2 films. Nature. 1991;353(6346):737–40.

77. Kaidashev EM, Lorenz M v, Von Wenckstern H, Rahm A, Semmelhack HC, Han KH, et al. High electron mobility of epitaxial ZnO thin films on c-plane sapphire grown by multistep pulsed-laser deposition. Appl Phys Lett. 2003;82(22):3901–3.

78. Han F, Kambala VSR, Srinivasan M, Rajarathnam D, Naidu R. Tailored titanium dioxide photocatalysts for the degradation of organic dyes in wastewater treatment: a review. Appl Catal A Gen. 2009;359(1–2):25–40.

79. Roy P, Berger S, Schmuki P. TiO2 nanotubes: synthesis and applications. Angewandte Chemie International Edition. 2011;50(13):2904–39.

80. Fujishima A, Honda K. Electrochemical photolysis of water at a semiconductor electrode. Nature. 1972;238(5358):37–8.

81. Hashimoto K, Irie H, Fujishima A. TiO2 photocatalysis: a historical overview and future prospects. Jpn J Appl Phys. 2005;44(12R):8269.

82. Joni IM, Nulhakim L, Vanitha M, Panatarani C. Characteristics of crystalline silica (SiO2) particles prepared by simple solution method using sodium silicate (Na2SiO3) precursor. In: Journal of Physics: Conference Series. IOP Publishing; 2018. p. 012006.

83. Karkare MM. Choice of precursor not affecting the size of anatase TiO2 nanoparticles but affecting morphology under broader view. Int Nano Lett. 2014;4(3):111.

84. Singh PK, Mukherjee S, Ghosh CK, Maitra S. Influence of precursor type on structural, morphological, dielectric and magnetic properties of TiO 2 nanoparticles. Cerâmica. 2017;63:549–56.

85. Chen X, Mao SS. Titanium dioxide nanomaterials: synthesis, properties, modifications, and applications. Chem Rev. 2007;107(7):2891–959.

86. Bade BR, Rondiya S, Bhopale SR, Dzade NY, Kamble MM, Rokade A, et al. Investigation of growth mechanism for highly oriented TiO 2 nanorods: the role of reaction time and annealing temperature. SN Appl Sci. 2019;1:1–13.

87. Parashar M, Shukla VK, Singh R. Metal oxides nanoparticles via sol–gel method: a review on synthesis, characterization and applications. Journal of Materials Science: Materials in Electronics. 2020;31(5):3729–49.

88. Bugalia A, Gupta V. Structural, morphological and spectroscopic studies of Bi–Ca co-doped SnTe. Journal of Materials Science: Materials in Electronics. 2023;34(33):2190.

89. Yang M, Kim D, Jha H, Lee K, Paul J, Schmuki P. Nb doping of TiO 2 nanotubes for an enhanced efficiency of dye-sensitized solar cells. Chemical Communications. 2011;47(7):2032–4.

90. Mor GK, Varghese OK, Paulose M, Shankar K, Grimes CA. A review on highly ordered, vertically oriented TiO2 nanotube arrays: Fabrication, material properties, and solar energy applications. Solar Energy Materials and Solar Cells. 2006;90(14):2011–75.

91. Gu F, Huang W, Wang S, Cheng X, Hu Y, Lee PS. Open-circuit voltage improvement in tantalum-doped TiO 2 nanocrystals. Physical Chemistry Chemical Physics. 2014;16(47):25679–83.

92. Shakeel Ahmad M, Pandey AK, Abd Rahim N. Advancements in the development of TiO2 photoanodes and its fabrication methods for dye sensitized solar cell (DSSC) applications. A review. Renewable and Sustainable Energy Reviews. 2017 Sep 1;77:89–108.

93. Archana PS, Gupta A, Yusoff MM, Jose R. Tungsten doped titanium dioxide nanowires for high efficiency dye-sensitized solar cells. Physical Chemistry Chemical Physics. 2014;16(16):7448–54.

94. Toriello M, Afsari M, Shon HK, Tijing LD. Progress on the fabrication and application of electrospun nanofiber composites. Membranes (Basel). 2020;10(9):204.

95. Wu X, Jiang QZ, Ma ZF, Fu M, Shangguan WF. Synthesis of titania nanotubes by microwave irradiation. Solid State Commun. 2005;136(9–10):513–7.

96. Matias ML, Morais M, Pimentel A, Vasconcelos FX, Reis Machado AS, Rodrigues J, et al. Floating TiO2-Cork Nano-Photocatalysts for Water Purification Using Sunlight. Sustainability. 2022;14(15):9645.

97. Ke W, Fang G, Wang J, Qin P, Tao H, Lei H, et al. Perovskite solar cell with an efficient TiO2 compact film. ACS Appl Mater Interfaces. 2014;6(18):15959–65.

98. Peng X, Chen A. Aligned TiO 2 nanorod arrays synthesized by oxidizing titanium with acetone. J Mater Chem. 2004;14(16):2542–8.

99. Kavan L, Tétreault N, Moehl T, Grätzel M. Electrochemical characterization of TiO2 blocking layers for dye-sensitized solar cells. The Journal of Physical Chemistry C. 2014;118(30):16408–18.

100. Lee S, Noh JH, Han HS, Yim DK, Kim DH, Lee JK, et al. Nb-doped TiO2: a new compact layer material for TiO2 dye-sensitized solar cells. The Journal of Physical Chemistry C. 2009;113(16):6878–82.

101. Noh JH, Lee S, Kim JY, Lee JK, Han HS, Cho CM, et al. Functional multilayered transparent conducting oxide thin films for photovoltaic devices. The Journal of Physical Chemistry C. 2009;113(3):1083–7.

102. Blešić MD, Šaponjić Z V, Nedeljković JM, Uskoković DP. TiO2 films prepared by ultrasonic spray pyrolysis of nanosize precursor. Mater Lett. 2002;54(4):298–302.

103. Xiaoyan D, Chengwu S, Yanru Z, Ni W. Hydrolysis preparation of the compact TiO2 layer using metastable TiCl4 isopropanol/water solution for inorganic–organic hybrid heterojunction perovskite solar cells. J Semicond. 2015;36(7).

104. Wu Y, Yang X, Chen H, Zhang K, Qin C, Liu J, et al. Highly compact TiO2 layer for efficient hole-blocking in perovskite solar cells. Applied physics express. 2014;7(5):052301.

105. Johnson RW, Hultqvist A, Bent SF. A brief review of atomic layer deposition: from fundamentals to applications. Materials today. 2014;17(5):236–46.

106. Kavan L, O'Regan B, Kay A, Grätzel M. Preparation of TiO2 (anatase) films on electrodes by anodic oxidative hydrolysis of TiCl3. Journal of Electroanalytical Chemistry. 1993;346(1–2):291–307.

107. Bahnemann DW. Mechanisms of organic transformations on semiconductor particles. In: Photochemical Conversion and Storage of Solar Energy: Proceedings of the Eighth International Conference on Photochemical Conversion and Storage of Solar Energy, IPS-8, held July 15–20, 1990, in Palermo, Italy. Springer; 1991. p. 251–76.

108. Sakthivel S, Shankar M V, Palanichamy M, Arabindoo B, Bahnemann DW, Murugesan V. Enhancement of photocatalytic activity by metal deposition: characterisation and photonic efficiency of Pt, Au and Pd deposited on TiO2 catalyst. Water Res. 2004;38(13):3001–8.

109. Turner M, Golovko VB, Vaughan OPH, Abdulkin P, Berenguer-Murcia A, Tikhov MS, et al. Selective oxidation with dioxygen by gold nanoparticle catalysts derived from 55-atom clusters. Nature. 2008;454(7207):981–3.

110. Ikram M, Umar E, Raza A, Haider A, Naz S, Ul-Hamid A, et al. Dye degradation performance, bactericidal behavior and molecular docking analysis of Cu-doped TiO 2 nanoparticles. RSC Adv. 2020;10(41):24215–33.

111. Kashale AA, Dwivedi PK, Sathe BR, Shelke M V, Chang JY, Ghule A V. Biomass-mediated synthesis of Cu-doped TiO2 nanoparticles for improved-performance lithium-ion batteries. ACS Omega. 2018;3(10):13676–84.

112. Rajamannan B, Mugundan S, Viruthagiri G, Praveen P, Shanmugam N. Linear and nonlinear optical studies of bare and copper doped TiO2 nanoparticles via sol gel technique. Spectrochim Acta A Mol Biomol Spectrosc. 2014;118:651–6.

113. Álvaro RJ, Diana ND, María AM. Effect of Cu on optical properties of TiO2 nanoparticles. Contemp Eng Sci. 2017;10(31):1539–49.

114. Choudhury B, Dey M, Choudhury A. Shallow and deep trap emission and luminescence quenching of TiO 2 nanoparticles on Cu doping. Appl Nanosci. 2014;4:499–506.

115. Rajendran V, Rajendran G, Karuppathevar N. Phtotocatalytic degradation of methyelene blue by Cu doped TiO2 thin films under visible light irradiation. Mechanics, Materials Science & Engineering Journal. 2017;9.

116. Kamble R, Mahajan S, Puri V, Shinde H, Garadkar K. Visible light-driven high photocatalytic activity of Cu-doped TiO2 nanoparticles synthesized by hydrothermal method. Mater Sci Res India. 2018;15(3):197–208.

117. Zhang W, Liu Y, Yu B, Zhang J, Liang W. Effects of silver substrates on the visible light photocatalytic activities of copper-doped titanium dioxide thin films. Mater Sci Semicond Process. 2015;30:527–34.

118. Bbumba S, Karume I, Nsamba HK, Kigozi M, Kato M. An Insight into Isotherm Models in Physical Characterization of Adsorption Studies. European Journal of Applied Sciences–Vol. 2024;12(2).

119. Guan B, Yu J, Guo S, Yu S, Han S. Porous nickel doped titanium dioxide nanoparticles with improved visible light photocatalytic activity. Nanoscale Adv. 2020;2(3):1352–7.

120. Li X, Wu Y, Shen Y, Sun Y, Yang Y, Xie A. A novel bifunctional Ni-doped TiO2 inverse opal with enhanced SERS performance and excellent photocatalytic activity. Appl Surf Sci. 2018;427:739–44.

121. Ajmal A, Majeed I, Malik RN, Idriss H, Nadeem MA. Principles and mechanisms of photocatalytic dye degradation on TiO 2 based photocatalysts: a comparative overview. RSC Adv. 2014;4(70):37003–26.

122. El Mragui A, Zegaoui O, da Silva JCGE. Elucidation of the photocatalytic degradation mechanism of an azo dye under visible light in the presence of cobalt doped TiO2 nanomaterials. Chemosphere. 2021;266:128931.

123. Wang B, Zhang G, Leng X, Sun Z, Zheng S. Characterization and improved solar light activity of vanadium doped TiO2/diatomite hybrid catalysts. J Hazard Mater. 2015;285:212–20.

124. Cao X, Liu C, Hu Y, Yang W, Chen J. Synthesis of N/Fe Comodified TiO2 Loaded on Bentonite for Enhanced Photocatalytic Activity under UV□Vis Light. J Nanomater. 2016;2016(1):8182190.

125. El Mragui A, Daou I, Zegaoui O. Influence of the preparation method and ZnO/(ZnO+ TiO2) weight ratio on the physicochemical and photocatalytic properties of ZnO-TiO2 nanomaterials. Catal Today. 2019;321:41–51.

126. El Mragui A, Zegaoui O, Daou I, Esteves da Silva JCG. Preparation, characterization, and photocatalytic activity under UV and visible light of Co, Mn, and Ni mono-doped and (P, Mo) and (P, W) co-doped TiO 2 nanoparticles: A comparative study. Environmental Science and Pollution Research. 2021;28:25130–45.

127. D'amato CA, Giovannetti R, Zannotti M, Rommozzi E, Ferraro S, Seghetti C, et al. Enhancement of visible-light photoactivity by polypropylene coated plasmonic Au/TiO2 for dye degradation in water solution. Appl Surf Sci. 2018;441:575–87.

128. Khan M, Xu J, Cao W, Liu ZK. Mo-doped TiO2 with enhanced visible light photocatalytic activity: a combined experimental and theoretical study. J Nanosci Nanotechnol. 2014;14(9):6865–71.

129. Cheng HE, Chen YR, Wu WT, Hsu CM. Effect of nitrogen doping concentration on the properties of TiO2 films grown by atomic layer deposition. Materials Science and Engineering: B. 2011;176(7):596–9.

130. Avilés-García O, Espino-Valencia J, Romero R, Rico-Cerda JL, Arroyo-Albiter M, Natividad R. W and Mo doped TiO2: synthesis, characterization and photocatalytic activity. Fuel. 2017;198:31–41.

131. Abushad M, Naseem S, Arshad M, Shafi A, Khan MZ, Ansari A, et al. Physical properties and photocatalytic activity of Cr□doped TiO2 nanoparticles. J Microsc. 2023;291(3):210–28.

132. Zhang J, Li M, Feng Z, Chen J, Li C. UV Raman spectroscopic study on TiO2. I. Phase transformation at the surface and in the bulk. J Phys Chem B. 2006;110(2):927–35.

133. Swamy V, Kuznetsov A, Dubrovinsky LS, Caruso RA, Shchukin DG, Muddle BC. Finite-size and pressure effects on the Raman spectrum of nanocrystalline anatase Ti O 2. Physical Review B—Condensed Matter and Materials Physics. 2005;71(18):184302.

134. de Lira SO, e Silva RL de S, Banerjee P, Franco Jr A. Effects of defect dipoles on the colossal permittivity of ambipolar co-doped rutile TiO2 ceramics. Journal of Physics and Chemistry of Solids. 2020;143:109456.

135. Deng QR, Xia XH, Guo ML, Gao Y, Shao G. Mn-doped TiO2 nanopowders with remarkable visible light photocatalytic activity. Mater Lett. 2011;65(13):2051–4.

136. Han X, Shao G. Electronic properties of rutile TiO2 with nonmetal dopants from first principles. The Journal of Physical Chemistry C. 2011;115(16):8274–82.

137. Guo M, Gao Y, Shao G. Complex doping chemistry owing to Mn incorporation in nanocrystalline anatase TiO 2 powders. Physical Chemistry Chemical Physics. 2016;18(4):2818–29.